Effect of magnetite nanoparticles on methanogenic degradation of *p*-cresol in anaerobic membrane bioreactor

By

Haochen Zhang

in partial fulfilment of the requirements for the degree of

Master of Science
in Civil Engineering

at the Delft University of Technology,
to be defended publicly on Tuesday September 17th, 2020 at 3:00 PM.

Thesis committee:
Jules van Lier, professor, Sanitary Engineering, TU Delft, NL
Henri Spanjers, associate professor, Sanitary Engineering, TU Delft, NL
David Weissbrodt, assistant professor, Environmental Biotechnology, TU Delft, NL
Joonyeob Lee, assistant professor, Environmental Engineering, Pukyong National University, KR
Ziwei Liu, PhD candidate, Tsinghua University, CN

This thesis is confidential and cannot be made public until December 31st, 2021.
An electronic version of this thesis is available at http://repository.tudelft.nl/

Acknowledgement

The end of my master student life at TU Delft is drawing near. The past two years have been by far the most joyful two years in my life. I have achieved bountiful personal growth, blended into a new culture, and made friends with amazing people. The journey would have been dull without these people.
Over the past nine months I have been working on this master thesis. Outbreak of Covid-19 occurred in the middle of this thesis work, which had a negative impact on the implementation of experimental plans, thus the delay of completion. It would have been impossible to complete the thesis work without the guidance provided by the thesis committee Jules van Lier, Henri Spanjers, David Weissbrodt, Joonyeob Lee and Ziwei Liu, as well as the support from the lab technicians Armand Middeldorp and Patricia van den Bos. I would like to especially express my gratitude to Joonyeob Lee, who introduced me the basics about the topic and about the lab work in the beginning two months, and Ziwei Liu, who offered detailed suggestions and guidance with her abundant theoretical knowledge and command of practical experience and was readily available to give a helping hand for the rest seven months of this thesis work. Finally, I would like to thank my family for the unconditional support of my study at TU Delft.

Abstract

Anaerobic membrane bioreactor (AnMBR) is a promising technology to treat phenolic wastewater. Conductive materials such as magnetite and granular activated carbon have been reported to be capable of improving anaerobic digestion by facilitating direct interspecies electron transfer (DIET). This research first investigated the effect of magnetite on the treatment of synthetic *p*-cresol (a relative abundant compound in phenolic wastewater) wastewater in a lab-scale AnMBR. Magnetite increased the reactor stability, permitted higher *p*-cresol loading rate in the AnMBR, and reduced the fouling potential of supernatant of the mixed liquor. Activities of dehydrogenase and F_{420} were significantly increased and this may have contributed to the enhanced reactor performance. Magnetite supplement did not have a substantial influence on the soluble microbial products (SMPs) concentration compared to the stage without magnetite whereas extracellular polymeric substances (EPS) concentration significantly increased with magnetite supplement. Reduced fouling potential of the supernatant of the mixed liquor may be attributed to the decrease of protein content in SMPs in the stage with magnetite supplement. Second, the effect of magnetite on the methanogenic degradation pathway of *p*-cresol was studied, in which the rate limiting step was the conversion of intermediate compound benzoate. Moreover, magnetite increased the maximum substrate degradation rate of all the chosen intermediates as well as the accumulative methane production. Batch test using inoculum adapted to magnetite failed to yield faster substrate degradation rate in comparison with the batch test using non-adapted inoculum. This may be ascribed to the loss of biomass when magnetite was removed from the collected sludge because magnetite and DIET-based microorganisms were closely associated and shaking manually was not sufficient for microorganisms to detach from the magnetite. Since magnetite nanoparticles enhanced reactor performance and stability as well as reduced fouling potential of the supernatant of the mixed liquor, potential commercial application of magnetite nanoparticles in AnMBR may permit shorter hydraulic retention time (HRT) and higher flux, which can lead to higher treatment capacity and lower operational costs. Further research should investigate the effect of potential magnetite corrosion on the reactor performance, the effect of magnetite on fouling potential of the mixed liquor, and likely loss of biomass in case of magnetite removal and methods to remove magnetite with as little loss of biomass as possible.

Contents

List of figures

List of tables

1. Introduction

1.1. Background information

In the context of combat against climate change, the Netherlands aims to transition to sustainable energy generation and consumption. The Dutch Waterschappen(Water Authorities) as well as Rijkswaterstaat attempt to achieve energy neutral operation within the organization themselves by the end of 2025 and 2030 respectively, and intend to contribute to the Dutch national goal to reaching energy neutral operation by 2050 (*Energie En Waterbeheer. Bouwstenen Voor de Energietransitie | STOWA*, n.d.). For instance, all Dutch households will have been cut off the supply of fossil fuels by 2050, among which is the natural gas extracted underground and supplied to households in order to heat buildings or for cooking. However, there still remains the need of natural gas for certain industries and buildings (*Energie En Waterbeheer. Bouwstenen Voor de Energietransitie | STOWA*, n.d.). Therefore new source of natural gas, namely biogas, has gained tremendous interest. Biogas is a mixture of methane, the major component of natural gas, and other gases which add to impurity. After removing the impurities, biogas can be upgraded to 'green gas' and can live up to the quality of natural gas (*Energie En Waterbeheer. Bouwstenen Voor de Energietransitie | STOWA*, n.d.). Biogas can be produced from anaerobic digestion of sludge or anaerobic treatment of wastewater, where influent chemical oxygen demand (COD) is partially removed and leaves the system in the form of methane.

Wastewater generated by certain chemical industries, such as coal gasification plants and pharmaceutical industries, contain high concentration of COD (Lin et al., 2012; Ozyonar & Karagozoglu, 2015), making them promising sources for biogas production. These water, however, poses challenges to the anaerobic treatment processes because of, among other things, the presence of toxic compounds. Characteristics of influent of a coal gasification water treatment plant (CGWTP) are shown in table 1.1 and table 1.2.

Table 1. 1 Characteristics of influent of a CGWTP, adopted from Wang et al. (2011)

Water quality index	Original wastewater
pH	9.8
Volatile phenols (mg/L)	2750
Non-volatile phenols (mg/L)	2660
Total phenols (mg/L)	5410
COD_{Cr} (mg/L)	21364

Table 1. 2 Composition of the influent of a CGWTP, adopted from Yang et al. (2006)

Organic compounds	Inlet concentration (%)
Phenol	7.05
Phenol, 4-methyl-	6.08
Phenol, 3,5-dimethyl-	2.94
Phenol, 2-[(trimethylsilyl)oxyl	4.95
Resorcinol	5.00
Phenol, 3-[(trimethylsilyl)oxyl	2.46
Phenol, 2,3-dimethyl-	0.41

Note: values represent the relative percentage of total peak area

Some anaerobic treatment technologies are capable of treating such types of industrial wastewater, among which is the anaerobic membrane bioreactor (AnMBR). AnMBR has advantages over other anaerobic treatment technologies because it can retain the slow growing microorganisms capable of degrading specific type of pollutants, allows higher concentration of mixed liquor suspended solids (MLSS), and does not depend on the formation of granular sludge (van Lier et al., 2015). It is therefore supposed to be a better technology among anaerobic treatment technologies for treating such types of industrial wastewater.

Recent studies have indicated that conductive materials such as carbon fibers and magnetite are capable of boosting direct interspecies electron transfer (DIET) between microbial communities. This could have implications on anaerobic digestion. A methane-producing anaerobic environment requires syntrophic cooperation between methanogenic archaea and other microorganisms, through which interspecies electron transfer takes place and enables methanogens to produce methane with the electrons transferred from other microorganisms in the form of H_2 or formate. Electrons can also be transferred directly, i.e. DIET. Some studies have been performed on the application conductive materials and the results show higher biogas production rate and higher permitted organic loading rate (OLR) in anaerobic digestion reactor (Dang et al., 2016; Lovley, 2017a, 2017b; Z. Zhao et al., 2018), implying application of conductive materials to anaerobic digestion could contribute to the goal of Dutch Water Authorities.

1.2. Knowledge gaps and problem statement

Based on previous research results, can conductive materials further improve the performance of AnMBR treating industrial wastewater from the abovementioned chemical industries. More specifically, can conductive materials achieve higher biogas

production rate and higher permitted OLR in an AnMBR? However, few previous studies were conducted to this end, and none was focused on whether conductive materials could improve the anaerobic digestion of *para*-cresol (*p*-cresol) in an AnMBR. *p*-cresol is of interest because of its relatively high abundance in the wastewater of coal gasification industry (W. Wang et al., 2011) as well as its toxic nature, whereas AnMBR is of interest is because, in addition to its advantages, it has been proved capable of treating saline phenolic wastewater (Muñoz Sierra et al., 2018; Muñoz Sierra et al., 2017).

The objective of this research is to investigate the effect of magnetite nanoparticles, a conductive material, on the treatment of *p*-cresol wastewater in an AnMBR. To achieve the objective, four research questions were addressed:

1) By how much can magnetite nano particles enhance methane production rate, COD removal efficiency, the substrate degradation rate in AnMBR treating *p*-cresol wastewater?

2) What is the DIET effect of magnetite nano particles on the fouling potential of mixed liquor during the digestion of *p*-cresol in AnMBR?

3) By how much can magnetite nanoparticles increase the methane production rate, COD removal efficiency and the substrate degradation rate when the anaerobic intermediates of *p*-cresol (4-hydroxybenzoate, benzoate, propionate) are used as the only substrates?

4) What is the optimal magnetite dosage that achieves the highest substrate degradation rate of AnMBR treating *p*-cresol?

2. Literature review

2.1. Phenolic wastewater

2.1.1. High toxicity of phenolic compounds in industrial wastewater

Phenolic compounds, or phenols, are chemical compounds with a hydroxyl group (-OH) directly bonded to an aromatic hydrocarbon group. While phenolic compounds are natural occurring substances of plants and microorganisms, or the product of decomposition of certain organic matters in nature, they can result from anthropogenic activities. For example they are present in larger quantity in the wastewater of coal gasification plants, coking plants, petroleum refineries, pharmaceutical, fertilizer and dye manufacturing plants, degreasing and painting stripping operations, fiberboard manufacturing and petrochemicals (Collins et al., 2005). The concentration of phenolic compounds in the these effluents varies from 10 to 17000 mg/L whereas the COD contributed by phenolic compounds consists of 40% to 80% of total COD (Veeresh et al., 2005). cresols are the common phenolic compounds found in these effluents, among which is *p*-cresol, an isomeric phenol with the para position substituted by a methyl group also known as 4-methylphenol. It is potentially carcinogenic, and can exert toxic effects on central nerve system, cardiovascular system, lung, kidney, and liver even at low concentration (Singh et al., 2008). In addition, it is toxic to aquatic life, and can lead to the degradation of ecosystems. A study on rats and mice showed that 30,000 ppm of *p*-cresol in the diet led to physiological changes, including increases in liver and kidney weights, deficits in liver function, bone marrow hypocellularity, irritation to the gastrointestinal tract and nasal epithelia, and atrophy of female reproductive organs (Andersen, 2006). Moreover, the US Environmental Protection Agency has designated phenol as a priority pollutant and regulates less than 1 ppb phenol is allowed in surface water. The toxicity level of phenol ranges between 9 and 25 mg/L for both human and aquatic life (Villegas et al., 2016). Therefore, concentrations of phenolic compounds should be reduced below the threshold value before industrial wastewater is discharged to receiving water bodies.

2.1.2. Superiority of biological treatment of phenolic wastewater

Various technologies have been applied to remove phenolic compounds from industrial wastewater. Whereas conventional methods include steam distillation, liquid-liquid extraction, adsorption, solid-phase extraction, wet air oxidation, catalytic wet air oxidation, and biodegradation, advanced methods refer to electrochemical oxidation, photo-oxidation, ozonation, UV/H_2O_2, Fenton reaction, membrane processes and

enzymatic treatment (Villegas et al., 2016). Among these methods, biological treatment is the most applied due to its robustness, low costs and simple design (Pradeep et al., 2015; Villegas et al., 2016). Both aerobic and anaerobic biological treatment are capable of degrading phenolic compounds. Jalayeri et al. showed acclimated activated sludge in a batch test was able to degrade phenol of 200 mg/L with optimal condition being 30°C and pH 7, while inhibition of microorganisms by phenol started to occur at 1500 mg/L phenol. Rafiei et al. (2014) compared the efficacy of hybrid membrane bioreactors (H-MBR) with conventional membrane bioreactors (MBR) treating synthetic phenolic wastewater at 1000 mg/L and found out that an H-MBR using polyurethane foam obtained the phenol removal rate of 99%, in comparison with 70.6% phenol removal rate achieved by conventional MBR, indicating bio-entrapped MBR performed much better than bio-film MBR. Rafiei et al. (2014) also concluded that and that H-MBR was able to recover from the shocks induced by sudden increase of phenol concentration from 1000 mg/L to 1250 mg/L and retrieve phenol removal, whereas conventional MBR failed to recover.

In a study of upflow anaerobic sludge blanket (UASB) reactor treating synthetic wastewater containing phenol and cresols (*m*-, *o*-, *p*- isomers), Veeresh et al. (2005) concluded that UASB could achieve more than 97% phenol removal rate at phenol concentration of 1260 mg/L and 3000 mg/L with 1:1 and 3:1 effluent recirculation respectively, that adding co-substrate such as glucose could also act as an strategy to maintain the phenol or cresol concentration within the inhibitory value, and that the degradability of phenol is more than that of *p*-cresol, which in turn is more than *m*- and *o*-cresol.

2.1.3. Pathway of methanogenic degradation of *p*-cresol

Anaerobic degradation of *p*-cresol have gained interests of researchers since 1980s. Studies have been performed on the degradation of *p*-cresol under denitrifying condition, sulphate reducing condition, iron reducing condition and methanogenic condition. However, the proposed pathways of anaerobic degradation of *p*-cresol even under the same condition diverged. For example, as shown in figure 2.1, under methanogenic conditions, Young & Rivera (1985) proposed *p*-cresol was initially demethylated to phenol. Next the ring was oxidized and cleaved, followed by anaerobic redox reaction till methane was formed in the final step.

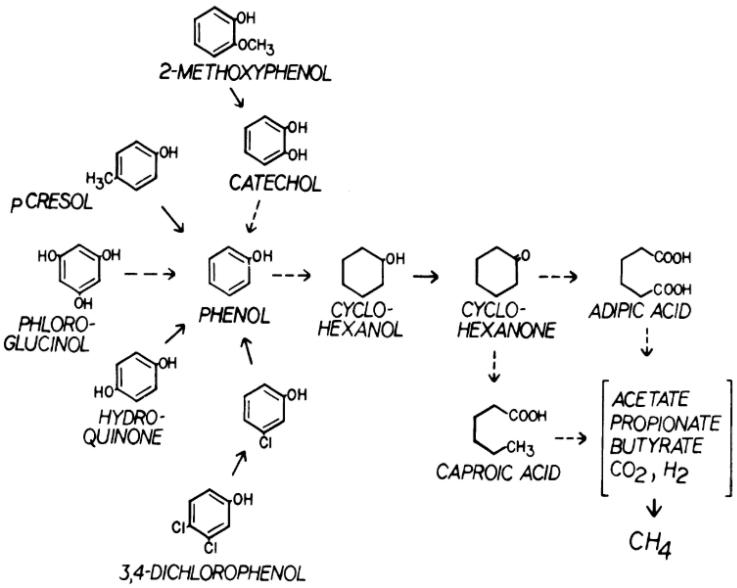

Figure 2. 1 Proposed methanogenic pathways of several substituted phenolic compounds, including *p*-cresol, adopted from Young & Rivera (1985)

However, different pathway under methanogenic conditions have been proposed by Häggblom et al. (1990). As shown in figure 2.2, *p*-cresol undergoes a completely different pathway until the ring is cleaved. The initial step is the oxidation of methyl group, to subsequent alcoholic hydroxyl group, aldehyde group and finally carboxyl group, followed by the dehydroxylation of the ring to form benzoate. Thereafter the ring will be oxidized and undergo ring fission. Q. Zhao & Liu (2016) proposed a methanogenic pathway similar to that of Häggblom et al. (1990), in which *p*-cresol first undergoes oxidation of methyl group, followed by dehydroxylation of the ring and subsequent ring cleavage.

A

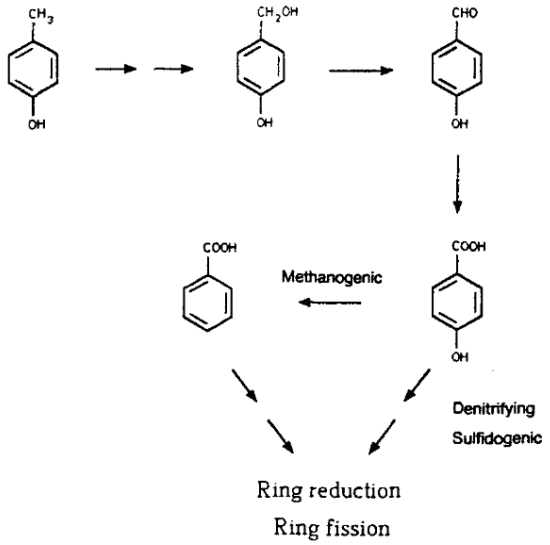

B

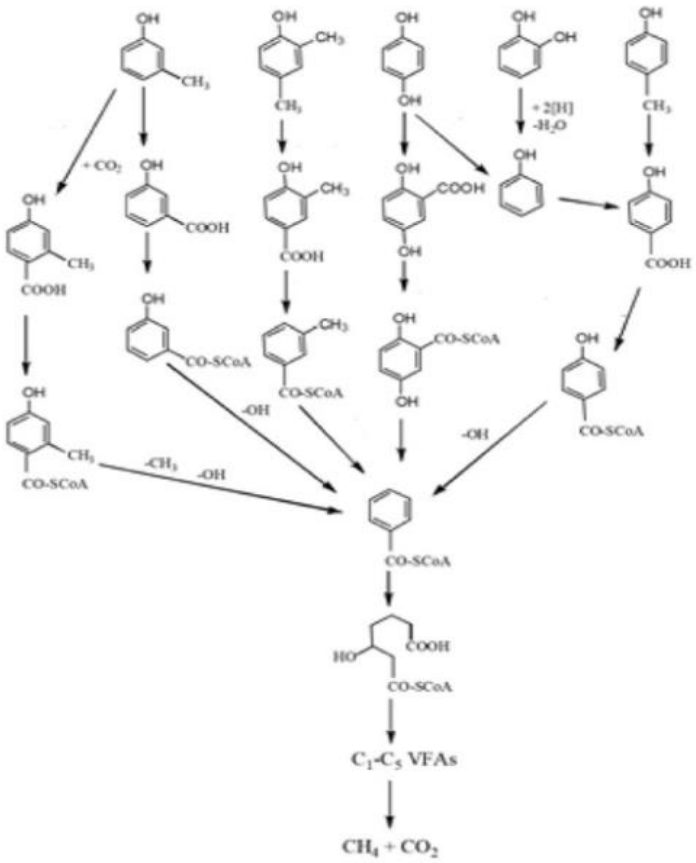

Figure 2. 2 A. Proposed methanogenic pathway of *p*-cresol under methanogenic condition, adopted from Häggblom et al. (1990); B. Proposed methanogenic pathways of some phenolic compounds found in CGWTP Q. Zhao & Liu (2016)

The different methanogenic pathways proposed are comprised of distinct intermediates, such as cyclo-hexanone versus benzoyl-CoA. Given that this research will utilize some of the intermediate compounds of methanogenic degradation of *p*-cresol, consensus is required. Other researched have indicated that benzoyl-CoA is the common central compound during the anaerobic degradation or anoxic degradation of aromatic compounds, among which *p*-cresol, as shown in figure 2.3.

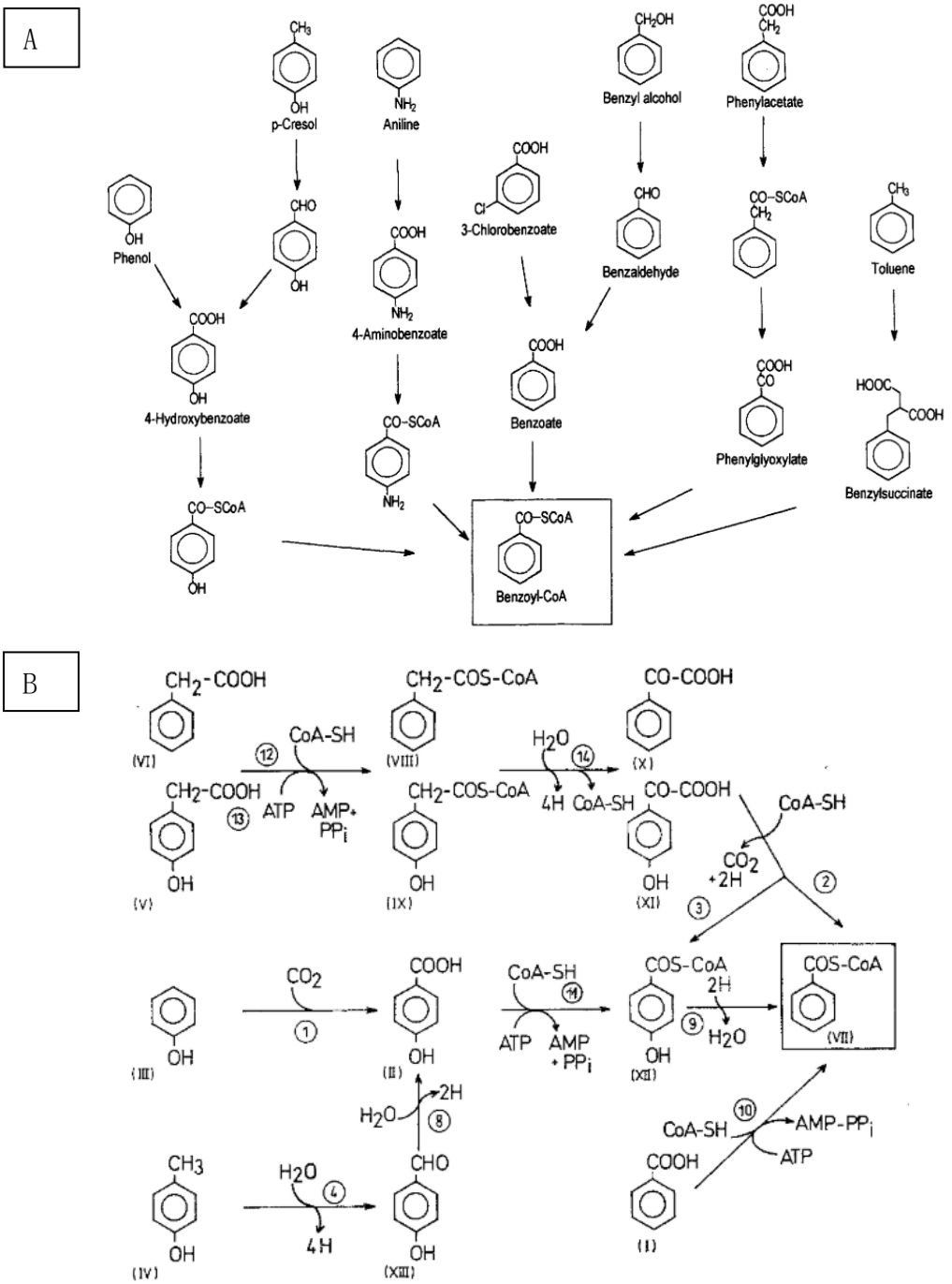

Figure 2. 3 Benzoyl-CoA as a central compound of anaerobic (A) and anoxic (B) degradation of aromatic compounds, adopted from Heider & Fuchs (1997) and Dangel et al. (1991) respectively

Therefore, it is plausible that, combining both the proposed methanogenic pathways and benzoyl-CoA as a central compound of anaerobic degradation of aromatic compounds, the methanogenic degradation of *p*-cresol is initiated by oxidation of the methyl group to carboxyl group, followed by dehydroxylation to form benzoyl-CoA, which undergoes ring fission short volatile fatty acids (VFAs) and eventually form acetyl-CoA and CO_2, as shown in figure 2.4.

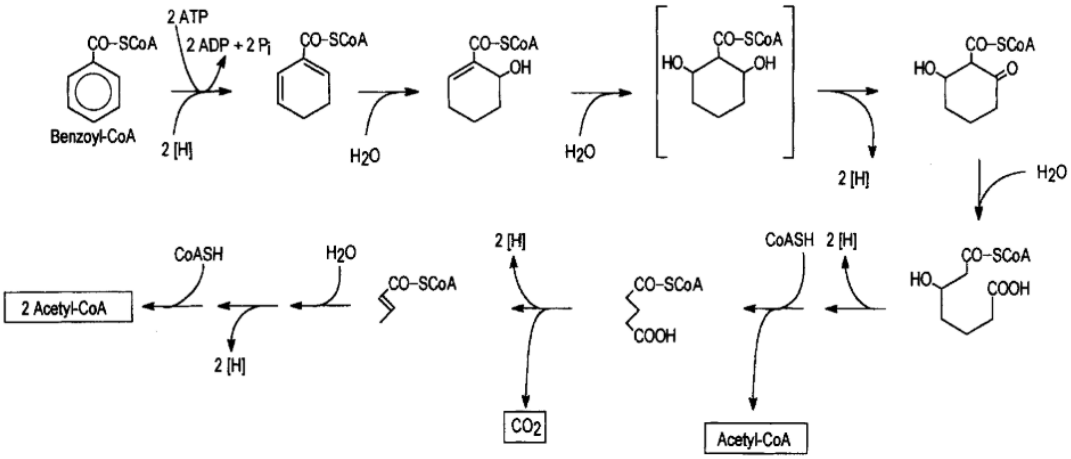

Figure 2. 4 Central anaerobic pathway leading from benzoyl-CoA to acetyl-CoA and on to CO_2, adopted from Heider & Fuchs (1997)

2.2. Anaerobic digestion

2.2.1. Widespread application of anaerobic digestion in wastewater treatment

Anaerobic digestion is a natural process that occurs at places with available organic matters and with low redox potential and (van Lier et al., 2020), such as some types of soil, certain sediments of lakes and oceans and municipal landfill. Anaerobic digestion has been used for treating wastewater from industries, pretreatment of high-strength wastes, treatment of domestic wastewater combined with aerobic processes. So far the most full-scale anaerobic technologies are applied to treating industrial wastewater (Abu-Orf et al., 2014).

Table 2. 1 Worldwide application of anaerobic technology for industrial wastewater treatment.
Total number of registered installed reactors = 2,266, according to a survey in January 2007, adopted from van Lier (2008)

Industrial sector	Type of wastewater	Number of reactors	Percentage(%)
Agro-food industry	Sugar, potato, starch, yeast, pectin, citric acid, cannery, confectionery, fruit, vegetables, dairy, bakery	816	36
Beverage	Beer, malting, soft drinks, wine, fruit juices, coffee	657	29
Alcohol distillery	Can juice, cane molasses, beet molasses, grape wine, grain, fruit	227	10
Pulp & paper industry	Recycle paper, mechanical pulp, NSSC, sulphite pulp, straw, bagasse	249	11
Miscellaneous	Chemical, pharmaceutical, sludge liquor, landfill leachate, acid mine water, municipal sewage	317	14

Compared to conventional aerobic technologies, anaerobic treatment of wastewater have the following advantages (van Lier et al., 2020):

- Significant reduction of sludge production and subsequent low costs of sludge handling and disposal
- Higher COD loading rate and resulting smaller reactor volume
- Much less energy required due to the absence of aeration
- Energy production in the form of biogas
- No or little requirement of additional dosage of chemicals
- Rapid start-up using granular anaerobic sludge as seed material
- Market value of excess sludge as seed material
- Potential recovery of unconsumed nitrogen and phosphate

2.2.2. Four successive steps of anaerobic digestion

The methane-producing anaerobic conversion of organic matters such as proteins, carbohydrates and lipids consists of four sequential steps: hydrolysis, acidogenesis, acetogenesis and methanogenesis. The entire conversion is not achieved by a single group of microorganism. Instead, the microbial consortia in such an environment are

comprised of a variety of microorganisms, each responsible for one or two steps in the entire chain. This is indicated in the figure 2.5 below.

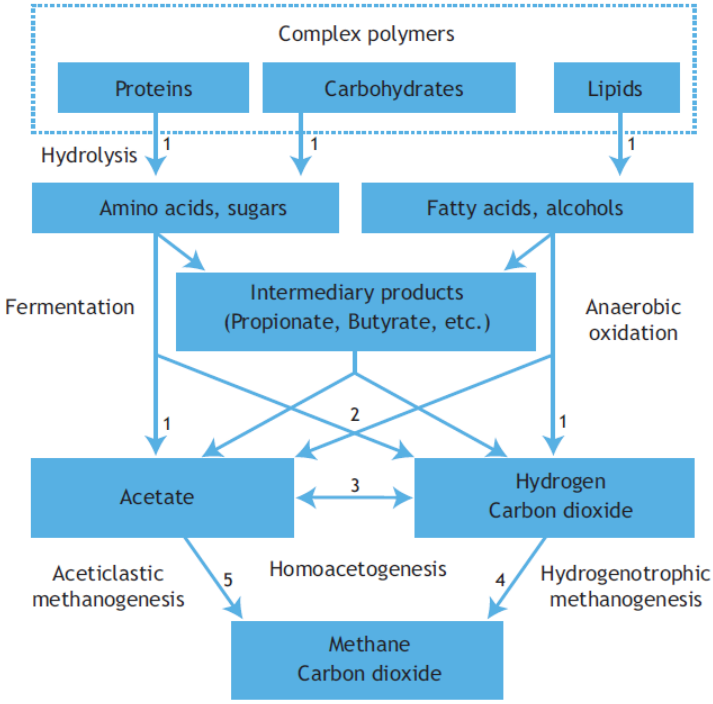

Figure 2. 5 Schematic representation of methane-producing anaerobic conversion of organic matters such as proteins, polysaccharides and lipids. Numbers represent the involved microorganism group: 1. Hydrolytic and fermentative bacteria; 2. Acetogenic bacteria; 3. Homo-acetogenic bacteria; 4. Hydrogenotrophic methanogens; 5. Acetoclastic methanogens, adopted from (Gujer & Zehnder, 1983; van Lier et al., 2020)

Hydrolysis is a process where polymers, such as proteins, polysaccharides and lipids, are degraded into simpler molecules, such as amino acids, simpler sugars and long chain fatty acids (LCFAs), by the extracellular enzymes excreted by the fermentative bacteria. The polymers are usually of particulate nature and need to be broken down to smaller soluble molecules before acidogenic bacteria can proceed with acidogenesis. Hydrolysis is regarded as the rate limiting step in anaerobic conversion since the available surface area of particulate polymers is limited due to low surface volume ratio (van Lier et al., 2020).

Acidogenesis occurs when hydrolyzed smaller molecules diffuse into the bacterial cells, where they will be anaerobically oxidized. The products depend on the substrates and circumstances (van Lier, 2018). Sucrose fermentation produces mainly acetate CO_2 and H_2 when the generated H_2 is scavenged by methanogens effectively, whereas it yields more reduced products such as ethanol, lactate, propionate, butyrate, CO_2 and H_2 when the H_2 accumulates (van Lier et al., 2020). Acidogenesis is the most rapid among four

steps because it yields the most energy for microbial growth in comparison with other three steps. Given that acidogenesis of sugars and lipids produces H^+, this process may cause acidification of the anaerobic reactor when the capacity of methanogenesis is exceeded. pH below the optimal range of methanogenesis will intoxicate methanogens, which leads to methanogens unable to degrade acetates and thus accumulation of VFAs and in turn exacerbates the acidification. This vicious circle can be illustrated in figure 2.6.

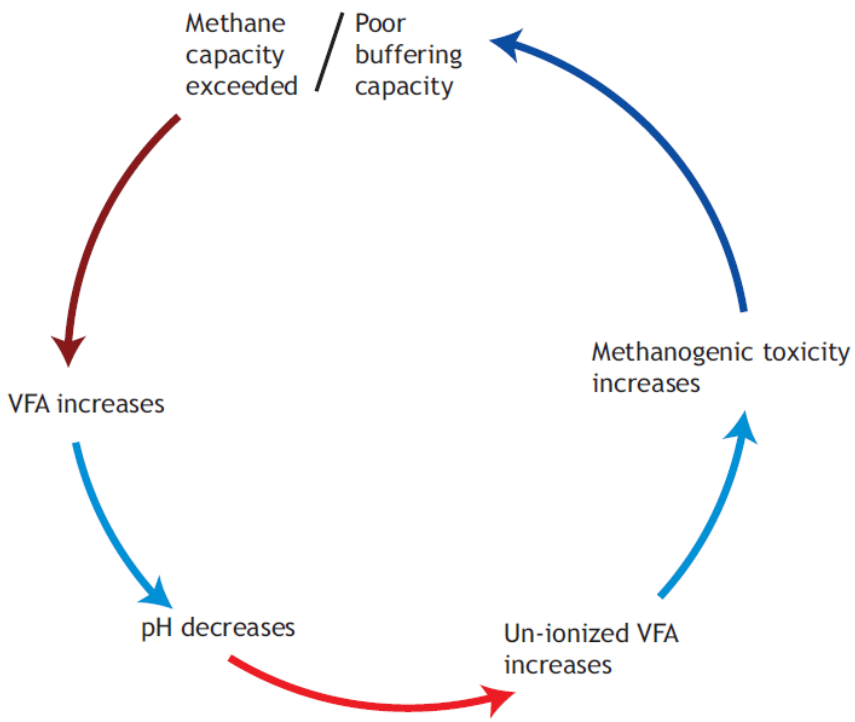

Figure 2. 6 Overloaded methanogenesis leads to acidified reactor in the manner of vicious circle, adopted from (van Lier et al., 2020)

Among the products of acidogenesis are the VFAs, which are the substrates (excluding acetate) involved in the third conversion step, acetogenesis. The products of acetogenesis are acetate, CO_2 and H_2. Thermodynamically speaking, the accumulation of H_2 renders the acetogenesis reactions unfavorable. Therefore H_2 scavengers such as methanogens play a key role in lowering the Gibbs free energy so that the reaction is exergonic and can occur spontaneously. However, if the partial H_2 pressure is too low, methanogenesis becomes thermodynamically unfavorable. Generally a partial H_2 pressure between 10^{-4} and 10^{-6} atm is essential for the stability of the anaerobic conversion process (van Lier et al., 2020).

The fourth and last step, methanogenesis, is where methanogens utilize substrates to form methane. The methanogens are classified into hydrogenotrophic methanogens, which use CO_2 and H_2 as substrate to form methane and water, and acetoclastic methanogens, which convert acetate into methane and water. Hydrogenotrophic and

acetoclastic conversions are shown in equation 1 and 2 respectively. CO_2/H_2 and acetate comprise of the majority of the methanogenic substrates.

$$CO_2 + 4H_2 \rightarrow CH_4 + 2H_2O \qquad \text{Eq. (1)}$$

$$CH_3COO^- + H_2O \rightarrow CH_4 + HCO_3^- \qquad \text{Eq. (2)}$$

2.2.3. Superiority of Anaerobic membrane bioreactor (AnMBR) in treating industrial wastewater under extreme conditions

There are various types of commercialized anaerobic reactor technology such as anaerobic contact process (ACP), anaerobic filter (AF), upflow anaerobic sludge blanket (UASB) reactor, fluidized-bed (FB) reactor, expanded granular sludge bed (EGSB) reactor, internal circulation (IC) reactor, anaerobic baffled reactor (ABR), and anaerobic membrane bioreactors (AnMBR) (Jules B Van Lier et al., 2020).

Recently AnMBR has received much research interest in the treatment of both municipal wastewater and industrial wastewater, due to the advantages resulting from coupling of membrane filtration and anaerobic digestion. On top of the advantages of anaerobic digestion, AnMBR can achieve total biomass retention, a key characteristic that enables AnMBR to outperform other anaerobic technologies in terms of smaller reactor size, effluent free of solids as well as the capability to treat certain types of industrial wastewater under extreme conditions which would otherwise cause failure to other anaerobic technologies (Lin et al., 2013; van Lier et al., 2020). However, a series of (potential) problems such as membrane fouling, discharges from industries containing toxic compounds, salinity, and increasing methane solubility in effluent with decreasing temperature, have posed challenges to application of AnMBR treating municipal wastewater, and thus so far no full-scale AnMBR has been applied to municipal wastewater (Ozgun et al., 2013).

In general AnMBR is based on two configurations: external/side-stream configuration and submerged/ immersed configuration, as shown in figure 2.7. The advantages of external configuration include better hydrodynamic control, easier replacement of the membrane and higher permissible fluxes. In comparison, submerged configuration requires less energy, less frequent cleaning and milder operational conditions (Lin et al., 2013).

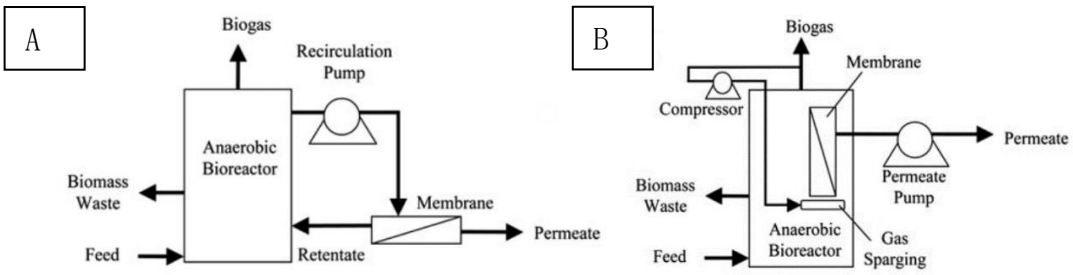

Figure 2. 7 Configurations of AnMBR: A. external/side-stream configuration, B. submerged/ immersed configuration, adopted from Dvořák et al., (2016)

Pilot studies of AnMBR treating municipal wastewater have shown that high COD removal efficiencies and low biosolids productions were achieved at hydraulic retention time (HRT) comparable to conventional aerobic processes under ambient temperatures. Furthermore, five out of nine pilot scale studies achieved a positive energy balance. However, in all nine pilot studies, fouling control remains the largest energy consumer in total energy balance, indicating that whether AnMBR can achieve net energy production for AnMBR unit itself largely depends on the energy consumption of fouling control (Shin & Bae, 2018).

Industrial wastewater is likely to be more frequently associated with extreme physicochemical conditions such as high salinity, high temperature, and presence of toxic compounds due to the trend of reduction in water consumption and increased water reuse (van Lier et al., 2020). These extreme conditions may cause failures in other anaerobic reactor technologies, whereas AnMBR is capable of treating industrial wastewater with high salinity and toxicants since AnMBR can retain special slow growing microorganisms capable of degrading toxic pollutants such as aromatic compounds under highly saline condition (Muñoz Sierra et al., 2018). Just like AnMBR treating domestic wastewater, AnMBR applying to industrial wastewater also has some issues: fouling and large energy consumption to maintain a mesophilic AnMBR treating industrial wastewater.

Improving biogas production in AnMBR may help achieve net energy production more easily. DIET has been suggested as one of the emerging strategies to improve anaerobic digestion in terms of higher biogas production rate and higher permissible maximum OLR (Barua & Dhar, 2017; Wu & Kim, 2020).

2.3. Direct interspecies electron transfer (DIET)

2.3.1. DIET between bacteria and methanogens

Successful syntrophy between methanogens and other microbes in an anaerobic environment essentially secures methanogenesis. This process essentially boils down to interspecies electron transfer (IET). IET can be achieved via two ways. The first is

via diffusion of electron carriers such as H_2 and formate, which are metabolites generated by some microbes but consumed by methanogens. This process can be relatively slow because it involves diffusion (Kato et al., 2012). The second IET is referred to as direct interspecies electron transfer (DIET), through which methanogens directly accept electrons from other species (Lovley, 2011). In comparison with diffusion of electron carriers, electron transfer via DIET is faster and results in more rapid conversion of organic waste to methane (Barua & Dhar, 2017).

DIET is a natural phenomenon and evidence of DIET between bacteria and methanogens was first found by Morita et al. (2011) in a UASB reactors treating brewery wastewater. DIET requires structures binding to membranes to physically connect and transfer electrons between two cells (Cheng & Call, 2016). Studies have suggested that c-type cytochromes (OmcS) and pili are the primarily responsible for DIET. Cytochromes are membrane-bound enzymes that can transfer electrons when cytochromes undergo oxidation and reduction. Pili are filamentous proteins which protrude from cell surface. Pili allow transfer of DNA between cells, assist cells with adhesion to surfaces, and facilitate mobility (Cheng & Call, 2016). Pili of some microbes exhibit conductivities comparable to that of metals, which may be caused by electron hopping between OmcS. This suggests DIET is essentially electron transfer along a succession of redox OmcS to electron acceptors with pili acting as a 'scaffold' (Cheng & Call, 2016). Schematic representation of IET mechanism is shown in figure 2.8 and figure 2.9.

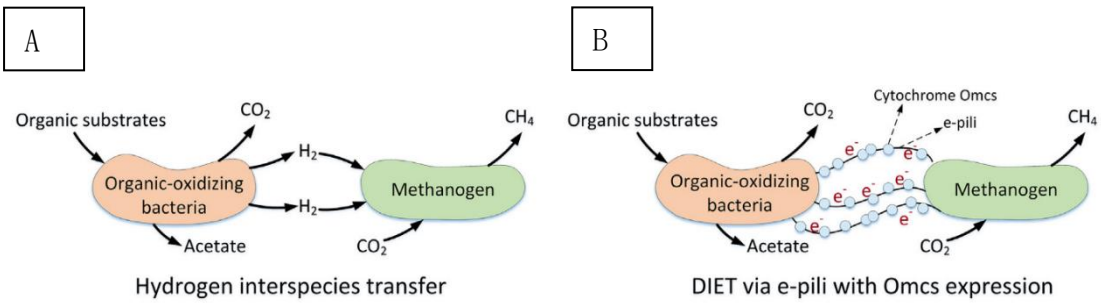

Figure 2. 8 Electron transfer via microbial metabolites such as H_2 (A) and via DIET (B), adopted from Yin & Wu (2019)

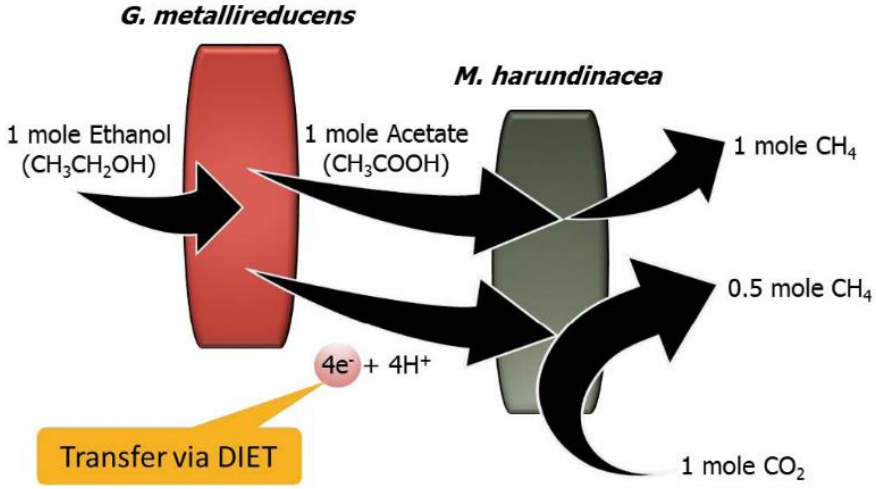

Figure 2. 9 Schematic picture of DIET based electron transfer between *G. metallireducens* to *M. harundinacea*, adopted from Barua & Dhar (2017)

2.3.2. DIET facilitated by conductive materials

Electrically conductive pili have mainly been found in *Geobacter* species. Furthermore, limited length of pili means aggregation of species is necessary for DIET (Cheng & Call, 2016). Because DIET is a more rapid and efficient way of electron transfer, many studies focused on facilitating DIET using artificial materials. Conductive materials such as granular activated carbon (GAC) and magnetite nanoparticles have been shown to be capable of inducing DIET among a wide range of bacteria which cannot produce pili as well as promoting DIET in anaerobic digestion (Barua & Dhar, 2017). As a result, anaerobic conversion was accelerated by the addition of conductive materials. For instance, research has shown syntrophic degradation of propionate and butyrate were improved by biochar and graphite (M. Zhang et al., 2019; Z. Zhao et al., 2016).
However, the mechanisms of conductive materials facilitating DIET vary, as shown in figure 2.10. *Geobacter* strains whose pili-coding genes were knocked out were still capable of DIET when GAC was added to the co-culture (Liu et al., 2012; Rotaru et al., 2014), proving conductive materials with large surface such as GAC and biochar can compensate the absence of pili. On the other hand, *Geobacter* species without OmsC-coding gene could achieve DIET in the presence of magnetite nanoparticles (Liu et al., 2015), indicating magnetite can substitute OmcS to promote DIET.

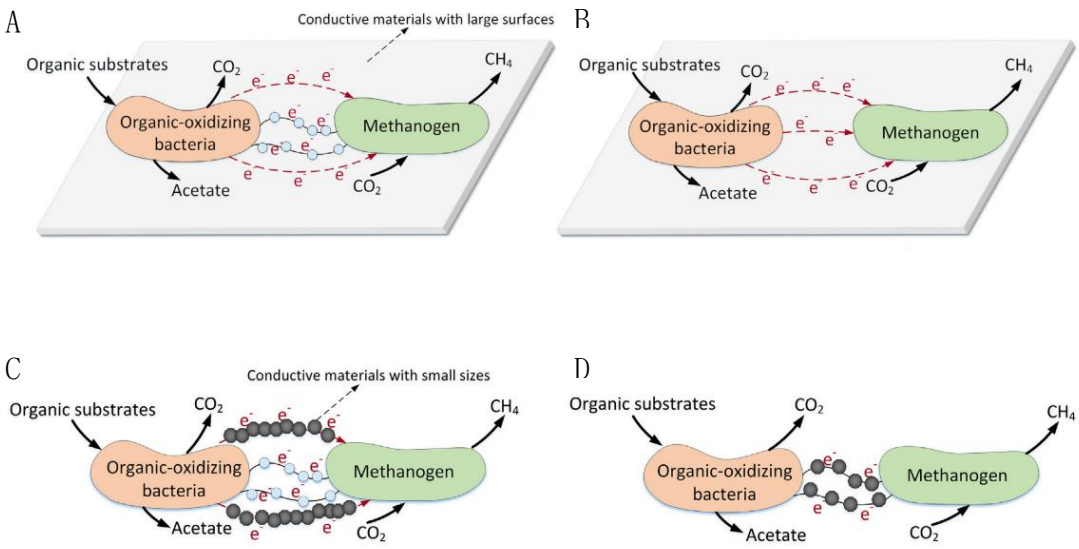

Figure 2. 10 Mechanisms of conductive materials facilitating DIET, adopted from Yin & Wu (2019):

A. Conductive materials with large surface, e.g. GAC and biochar, promoting DIET;

B. Conductive materials with large surface compensating the deficiency of pili and OmcS;

C. Conductive materials with small size, e.g. magnetite nanoparticles, promoting DIET;

D. Conductive materials with small size compensating the deficiency of OmcS

3. Materials and methods

3.1. AnMBR

3.1.1. Reactor configuration and operation

A lab-scale AnMBR was used for experiments. The schematic drawing is shown in figure 3.1. The reactor was maintained at an effective volume of 6 L. A tubular ultrafiltration membrane module (X-flow compact 33, Pentair, the Netherlands) with 5.2 mm diameter was configured in a side-stream configuration. Trans-membrane pressure was monitored by three sensors (ATM-800, AE sensors, the Netherlands). Influent flow was provided at 1.5 L/d by a peristaltic pump (120U, WATSON MARLOW). Mixed liquor between bioreactor and membrane module was recirculated at 1800 L/d by another peristaltic pump (620U, WATSON MARLOW) to achieve complete mixing and membrane fouling controlling. A pH sensor (Memosens, Germany) and a temperature sensor (ATM-800, AE sensors, the Netherlands) were plugged into the reactor and submerged in the mixed liquor to monitor the real-time pH and temperature. The water bath (Tamson instruments, the Netherlands) provided a constantly recirculated flow on the periphery of the AnMBR to maintain a temperature of 37 ℃ of the mixed liquor.

In phase 1, *p*-cresol concentration in the feed was stepwise increased until the reactor failed, when gas production decreased to 0 and COD concentration of the permeate increased sharply. Thereafter *p*-cresol loading was decreased to the initial value of phase 1, i.e. 300 mg/L, and 20 mmol/L magnetite nanoparticles with between 50 nm and 100 nm particle size (SIGMA-ALDRICH) was added to the reactor because it was reported as the optimal dosage (Lee et al., 2019). Magnetite concentration was maintained at 20 mmol/L by supplementing the amount of magnetite taken out along with mixed liquor sampling. When gas production was detected, experiment was moved to phase 2 to and *p*-cresol concentration in the feed was stepwise increased in the same manner as in phase 1. Table 3.1 gives an overview of the operation conditions, where phase 1 is defined as the stage without magnetite supplement and phase 2 as the stage with magnetite supplement.

Permeate was collected every other day, filtered with 0.45 μm filter (Chromafil®) for COD analysis using Hach Lange kits and VFA analysis using gas chromatograph (Agilenttech 7890A). Gas production was measured daily by a gas counter (R1-CH4, Ritter Apparatebau) connected to the headspace, whereas biogas composition was measured using gas chromatograph (Agilenttech 7890A).

Mixed liquor was collected once a week for COD and VFA analysis, first centrifuged at 12000 rpm (ST16R, Thermo Scientific) for 5 min before getting filtered. Analyses were performed in the same way as the permeate.

Total suspended solids (TSS) and VSS were analyzed once a week. Filter paper placed in an aluminum dish was dried in an oven (Memmert) at 105 °C for 24 hours and weighed on a balance (Mettler AE 200). Then the filter paper with the aluminum dish was stored in a desiccator. The filter paper was placed on a vacuum flash. 2 mL mixed liquor was transferred on the filter paper and vacuum-filtered. Triplicate measurements were performed. The filter paper with the aluminum dish was then dried in oven at 105 °C for 24 hours and then in a desiccator before weighed. After weighing the filter paper with the aluminum dish was transferred to a muffle oven (Nabertherm, Airtemp heattechnology) and burned at 550 °C. Finally the dish was dried in the desiccator and weighed.

3.1.2. Inoculum and composition of synthetic *p*-cresol wastewater

Inoculum of the AnMBR was collected from a full-scale UASB reactor treating industrial wastewater (Shell, Moerdijk, The Netherlands). *p*-cresol and yeast extract concentration were stepwise increased (see table 3.1.) while acetate concentration remained fixed in the synthetic wastewater. Sodium concentration was maintained at a fixed level of 7.57 g Na^+ /L. Buffer solution K_2HPO_4 and NaH_2PO_4 as well as micro- and macronutrients were supplied. More detailed information of the composition of the synthetic *p*-cresol wastewater is attached in the Appendix.

Table 3. 1 Operation conditions of AnMBR

Phase		Day	OLR ($gCOD \cdot L^{-1} \cdot d^{-1}$]	*p*-cresol (g *p*-cresol$\cdot L^{-1} \cdot d^{-1}$)	Magnetite (mmol/L)
1	1.1	0-12	0.73	0.3	0
	1.2	12-24	0.93	0.6	
	1.3	24-81	1.33	1.2	
	1.4	81-94	1.60	1.6	
	1.5	94-108	1.86	2.0	
	1.6	108-122	2.13	2.4	
	1.7	122-129	2.39	2.8	
2	2.1	0-14	0.73	0.3	20 mmol/L
	2.2	14-28	0.93	0.6	
	2.3	28-56	1.33	1.2	
	2.4	56-70	1.60	1.6	
	2.5	70-84	1.86	2.0	
	2.6	84-98	2.13	2.4	
	2.7	98-112	2.39	2.8	

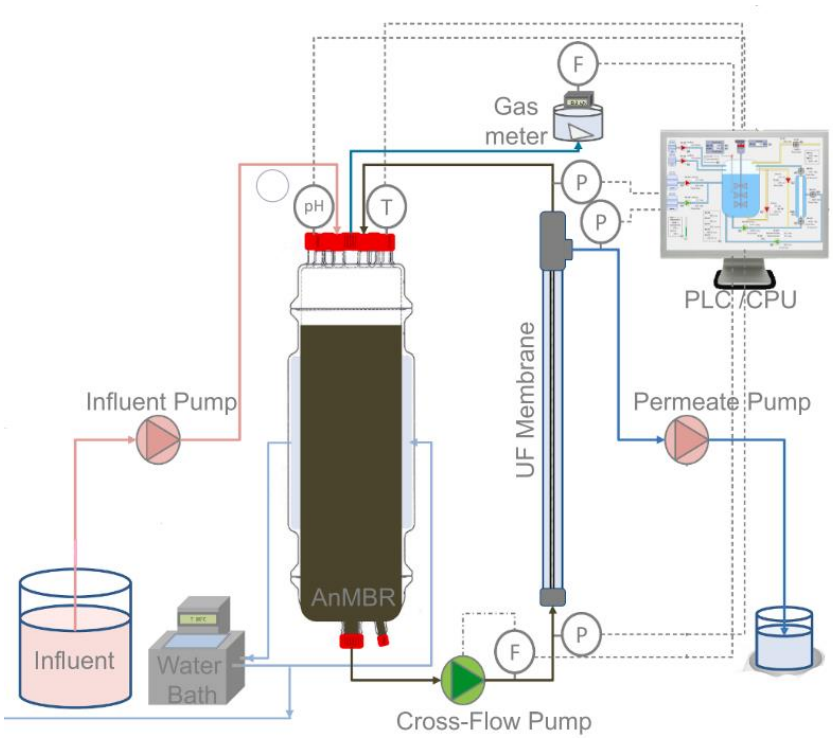

Figure 3. 1 Schematic drawing of reactor setup, adopted from Muñoz Sierra et al. (2019)

3.1.3. Fouling potential measurement of supernatant

100 mL mixed liquor was collected during each phase for fouling potential analysis and for mixed liquor property analysis. For fouling potential analysis, the mixed liquor was first centrifuged at 4 ℃, 8000 rpm for 10 minutes. Supernatant was collected and diluted with 1× phosphate buffer solution to 120 mg COD/L. The diluted supernatant was transferred to a stirred cell (Amicon Stirred Cell Model 8050, EMD Millipore, Germany) placed on a magnetic stirrer with 120 rpm. Trans membrane pressure was provided by nitrogen gas at 20 kPa. 0.45 μm cellulose acetate membranes (Whatman) was used. Change of mass of permeate was automatically documented by a balance (KERN EWJ) connected to the computer.

3.1.4. Mixed liquor property analysis

To analyze mixed liquor property, extra cellular substances (EPS) and soluble microbial products (SMPs) were extracted following the method described by Morgan et al. (1990). Total organic carbon (TOC) of EPS was analyzed using Hach Lange kits, and spectrophotometer (Hach Lange DR3900). Polysaccharides of EPS were measured with phenol-sulfuric acid method described by Dubois et al., 1956). Proteins of EPS were measured with Coomassie protein assay (SIGMA-ALDRICH). Polysaccharides and proteins of SMPs were also measured with the same methods. Dehydrogenase was analyzed according to the method modified from Xie et al. (2014). Coenzyme F_{420} was analyzed based on the methods described by Tian et al. (2017). Humic like substances were analyzed using the modified Lowry method described by Frølund et al. (1995). Statistical analysis were performed using SPSS.

3.2. Batch experiments about *p*-cresol degradation pathway

3.2.1. Overview of the batch experiments

Two Batch experiments about p-cresol degradation pathway, one using inoculum not having adapted to magnetite and the other using inoculum having adapted to magnetite, were conducted using *p*-cresol, 4-hydroxybenzoic acid (4HBA), benzoic acid (BA) and propionic acid as starting substrate. Furthermore, 2-bromoethanesulfonate (BES) and magnetite were supplemented in different groups. The schematic plan of the batch experiments is shown in figure 3.2 below. Detailed addition of chemicals of the batch experiments can be found in Appendix. All serum bottles were performed in duplicate measurements.

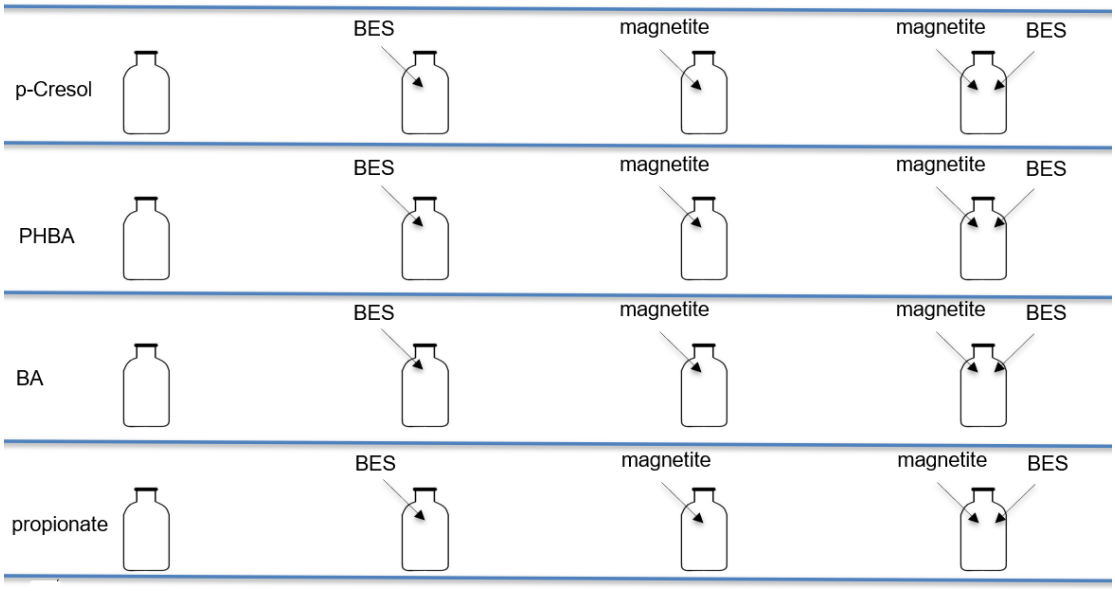

Figure 3. 2 Schematic drawing of the plan of batch experiments about p-cresol degradation pathway

3.2.2. Preparation of the batch experiments

The first batch experiment used inoculum collected from AnMBR at the end of phase 1.3 shown in table 3.1, while the second batch experiment used inoculum collected at the end of phase 2.3 shown in table 3.1. Before inoculation, sludge collected during phase 1.3 was cleansed. Sludge was centrifuged at 10000 rpm for 10 minutes. Supernatant was discarded and 1× phosphate buffer solution was added to reach the same volume before supernatant was discarded. The sediment was mixed well and centrifuged once again at 10000 rpm for 10 minutes. Thereafter the supernatant was discarded and sediment was resuspended by 1× phosphate buffer solution and centrifuged once again at 10000 rpm for 10 minutes. Suspended inoculum was then ready.

Sludge collected during phase 2.3 was first shaken intensely manually. Thereafter magnetite nanoparticles were removed by a magnetic bar. The sludge left was subjected to the same cleansing procedure as mentioned in the previous paragraph. Then inoculum and other agents were transferred to the serum bottles so that the initial volatile suspended solids (VSS) concentration was 1 g/L and total liquid volume in the serum bottles was 80 mL. The serum bottles were sealed by a stopper and a crimp cap and flushed with nitrogen gas for 5 minutes. All bottles were incubated at 120 rpm and 37 °C (New Brunswick™ Innova® 44).

3.2.3. Measurements of parameters

Gas production was monitored daily by a 10 mL glass syringe (FORTUNA OPTIMA, LUER) after the serum bottles were cooled down to room temperature (20 °C) in a water bath. Gas in the glass syringe was not injected back into the serum bottles. Gas composition was measured once a week by taking 1 mL gas sample in the headspace with 1 mL plastic syringe (Terumo) and injecting into the gas chromatograph. 1 mL mixed liquor was sampled every other day from the serum bottles, filtered by 0.45 μm filter and prepared for the substrate as well as VFA measurement in the gas chromatograph. 4HBA concentration was detected by a liquid chromatograph (SHIMADZU). In case of gas and liquid sampling, nitrogen gas was injected into the serum bottles by the glass syringe to maintain the pressure in the serum bottles. When the Batch experiments were terminated, TSS and VSS were analyzed according to the method described in section 3.1.1 and mixed liquor property was analyzed in the same manner as described in section 3.1.3.

Experimental data of substrate degradation were then fitted with the modified Gompertz model (J. Li et al., 2005) and Logistic model (J. Li et al., 2005; Zwietering et al., 1990) using Python curve fitting function which also gave the degree of curve fitting. Python code is attached in the Appendix. Modified Gompertz model and Logistic model are shown in equation 3 and 4 respectively:

$$S = S_0 \times \{1 - e^{\left\{-e^{\left[\frac{R_m e}{S_0}(\lambda - t) + 1\right]}\right\}}\} \qquad (3)$$

$$S = S_0 \times \{1 - \frac{1}{1 + e^{\left[\frac{4R_m}{S_0}(\lambda - t) + 2\right]}}\} \qquad (4)$$

where S is the substrate concentration, S_0 the initial substrate concentration, R_m the maximum substrate degradation rate, λ the lag phase time, and t the incubation time, e is Euler's number.

3.3. Optimization of magnetite dosage

Batch tests were performed at 0, 10, 20, 30, 40, 50, 75, 100, 200 mmol/L magnetite. Duplicate measurements were performed. Two abiotic group, one with no magnetite addition the other with 200 mmol/L, were also prepared (no inoculum of sludge) and no replicate was applied. Inoculum collected from reactor phase 1.3 was used and underwent the same treatment as described in section 3.2.2, so did the addition of inoculum, chemicals, liquid volume, sealing, and nitrogen gas flushing.

Measurements of gas production, gas composition, substrate as well as VFA concentration, and TSS/VSS were also conducted in the same manner as described in section 3.2.3. Mixed liquor property and curve fit were not performed.

4. Results and discussion

4.1. AnMBR

4.1.1. Enhanced reactor performance possibly due to supplement of magnetite nanoparticles

Effluent composition of the AnMBR during phase 1 and phase 2 is shown in figure 4.1.1 *p*-cresol as well as some anaerobic intermediate products of *p*-cresol were monitored. During phase 1 the reactor failed when the *p*-cresol loading rate was increased to 0.7 $g \cdot L^{-1} \cdot d^{-1}$, as evidenced by the sharp increase of *p*-cresol concentration from day 124 to day 130 as well as the increase of acetate concentration from day 130 to day 140, and the sharp decrease of oxidation reduction potential (ORP) shown in figure 6.1 in appendix. In comparison, during phase 2 the AnMBR was still well functioning when the *p*-cresol loading rate was increased to 0.7 $g \cdot L^{-1} \cdot d^{-1}$, as evidenced by the nearly 0 concentration of *p*-cresol and VFAs in the effluent, indicating magnetite may have improved the maximal *p*-cresol loading rate that the reactor could handle.

Higher permissible OLR when applying conductive materials to anaerobic digestion was found by other researchers. Wang et al. (2019) reported at least 33.33% higher permissible OLR in a lab-scale EGSB supplemented with magnetite nanoparticles compared to the control group without magnetite addition treating synthetic sucrose wastewater. Lei et al. (2016) reported that a lab-scale UASB supplied with carbon cloth treating fresh leachate from a municipal solid waste incineration plant yielded a 34% higher OLR in comparison with a control UASB reactor without carbon cloth.

When the *p*-cresol loading rate was increased from 0.15 $g \cdot L^{-1} \cdot d^{-1}$ to 0.3 $g \cdot L^{-1} \cdot d^{-1}$ in phase 1 (day 25), reactor experienced a shock period, evidenced by the increase of *p*-cresol concentration from day 25 to day 49. In phase 2, however, this shock period was not observed (day 28). This suggests magnetite may have improved the resistance of the reactor to sharp change of *p*-cresol loading and thus could increase the process stability. Enhanced reactor stability may have resulted from a change in microbial community, which shifted to one with more abundant bacteria and methanogens capable of DIET (Lei et al., 2018).

Enhanced process stability is consistent with the findings of Baek et al. (2017), who showed that an anaerobic continuously stirred tank reactor (CSTR) supplemented with magnetite treating dairy effluent could better resist the increased concentration of ammonium, showing much smaller or no fluctuation of effluent COD compared to the reactor without magnetite.

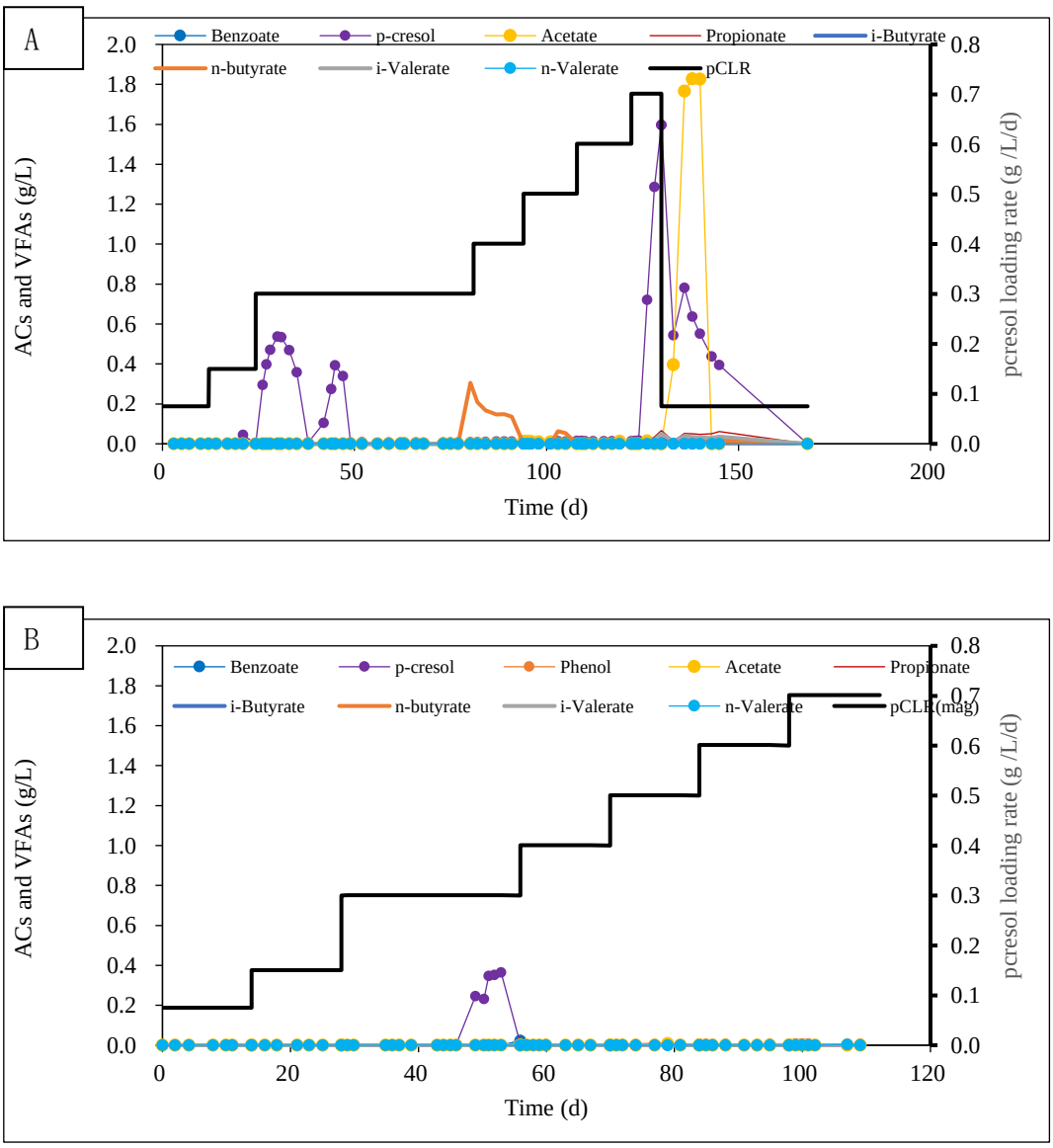

Figure 4.1.1 Effluent composition of the AnMBR, A: phase 1 without magnetite; B: phase 2 with magnetite

From day 63 to day 81 in phase 1.3 100 mL biomass was sampled every day, whereas from day 38 to day 46 in phase 2.3 a total of 1170 mL biomass was collected for batch experiments, coinciding with the increase of n-butyrate at the end of phase 1.3 and increase of p-cresol at the end of phase 2.3 respectively. This was caused by the decrease in VSS concentration in phase 1 from day 66 and in phase 2 from day 42, as

shown in figure 4.1.2. When the reactor was functioning well, VSS concentration fluctuated and did not show a specific trend. However during phase 1.7 where microorganisms were inhibited, VSS concentration showed a decreasing trend.

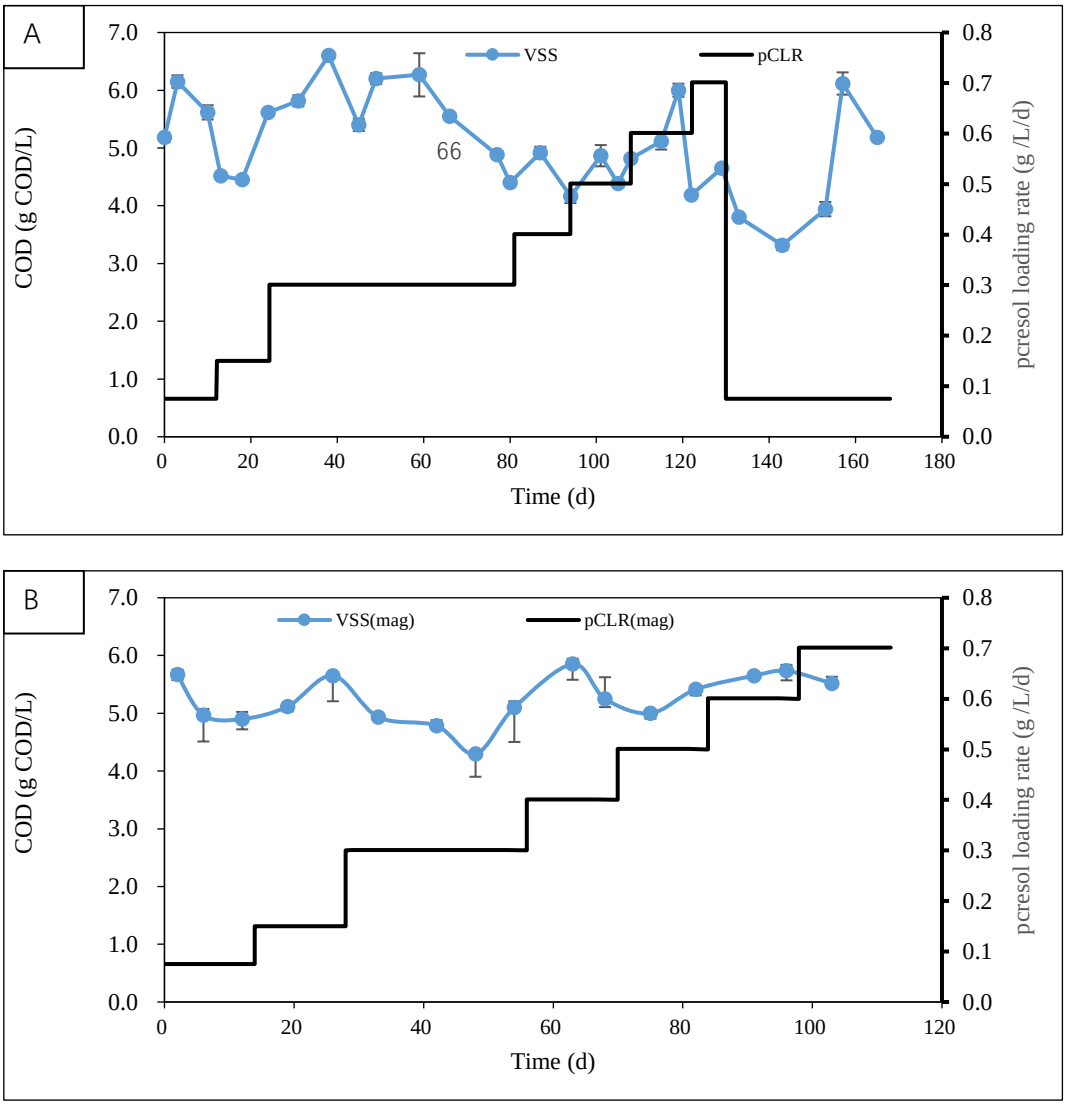

Figure 4.1.2 VSS composition of the AnMBR, A: phase 1 without magnetite; B: phase 2 with magnetite. The error bar represents the standard deviation of the triplicate measurements

Permeate COD shown in figure 4.1.3 below coincides with the shock period during phase 1.3 (increase of permeate COD), reactor failure during phase 1.7 (sharp increase of permeate COD), and stable reactor performance throughout phase 2 (well-functioning during phase 2.7) except at the end of phase 2.3, as discussed above.

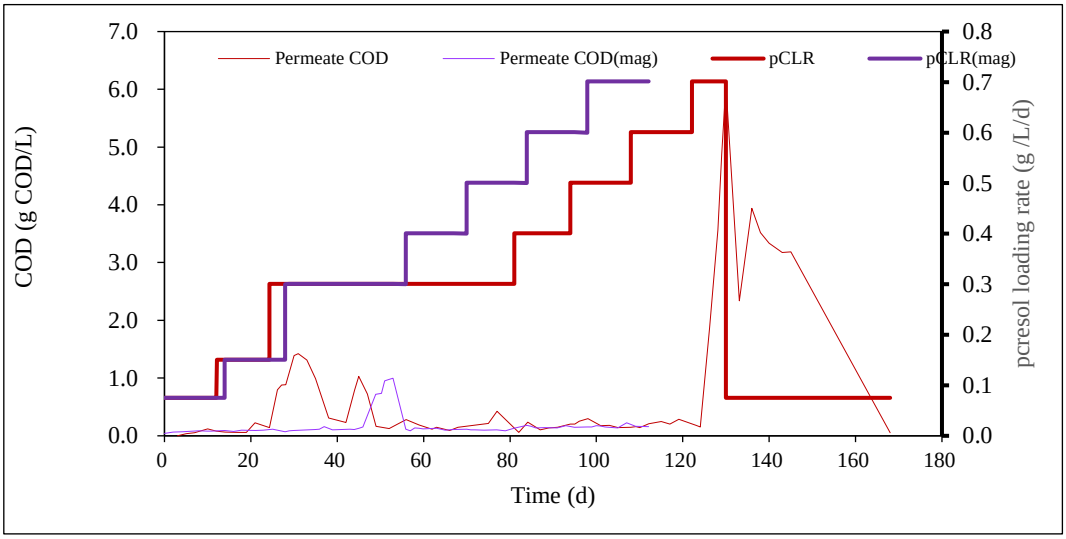

Figure 4.1.3 Permeate COD of the AnMBR, phase 1 without magnetite and phase 2 with magnetite

Specific methane production is given in figure 4.1.4, which also shows shock period during phase 1.3 (decrease of specific methane production), reactor failure during phase 1.7 (specific methane production decreasing to 0) and stable reactor performance throughout phase 2 (stable specific methane production during phase 2.7) except at the end of phase 2.3, as discussed above. Specific methane production in both phase 1 and 2 showed an increasing trend with the increase of *p*-cresol loading rate when the reactor well functioned. This increasing specific methane production trend is expected because the VSS and COD removal efficiency shown in figure 4.1.2 and 4.1.5 respectively overall remained stable when the *p*-cresol loading rate increased, suggesting more COD was conserved in the form of CH_4.

On the other hand, specific methane production of both phases under same *p*-cresol loading rate remained approximately the same, indicating magnetite may not improve the specific methane production under the same *p*-cresol loading rate during both phases. This is expected because the COD removal efficiency was above 95% during both phases and VSS concentration was in general stable when the reactor was well functioning, suggesting similar amount of COD was converted to CH_4, thus yielding a similar specific methane production.

While no improvement of methane production due to magnetite supplementation was observed in this research, other researchers reported the enhanced methane production. For instance, magnetite supplementation increased methane production by 16.1% in anaerobic digestion treating swine manure (J. Zhang et al., 2019). Cruz Viggi et al. (2014) observed methane production enhanced up to 33% by supplementation of magnetite when studying methanogenic propionate degradation. However, study of the effect of GAC supplementation on mesophilic and thermophilic anaerobic digestion showed different results: although methane productivity was increased by GAC in

mesophilic condition, thermophilic digestion with GAC addition did not yield methane productivity enhancement, suggesting enhanced process kinetics under thermophilic condition offset the effect of GAC (Ryue et al., 2019). Similar to the thermophilic condition which failed to enhance methane productivity, this research also did not observe enhanced specific methane productivity as explained by the observation that when the reactor functioned well, COD removal efficiency remained about 95% in both phases and VSS concentration remained stable, indicating similar amount of COD was converted to methane by similar amount of biomass, thus no enhanced methane productivity.

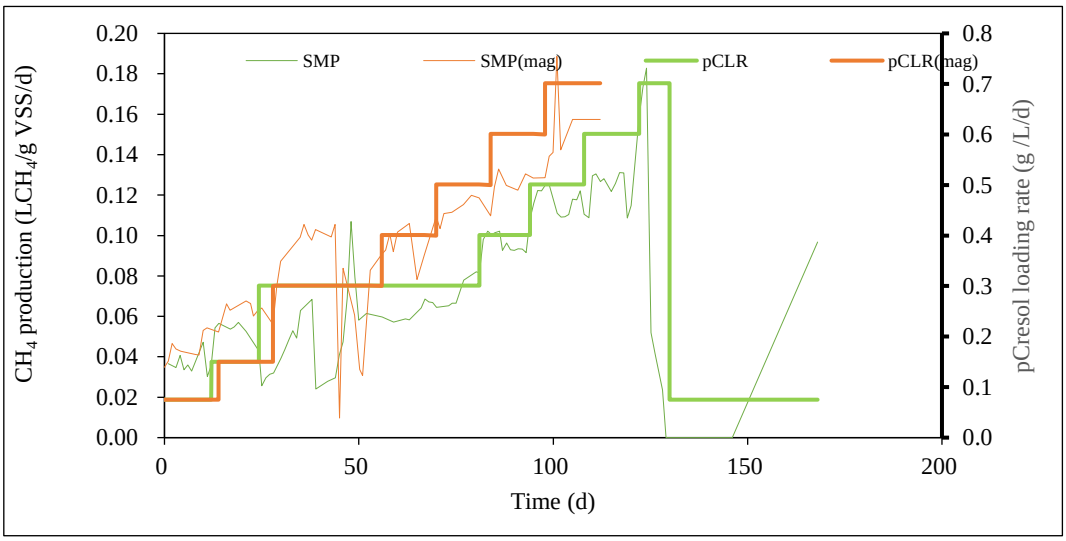

Figure 4.1.4 Specific methane production of the AnMBR during phase 1 without magnetite and phase 2 with magnetite

COD removal efficiency is given in the figure 4.1.5, which also shows the shock period during phase 1.3 (decrease of COD removal efficiency), reactor failure during phase 1.7 (COD removal efficiency decreasing to 0) and stable reactor performance throughout phase 2 (stable COD removal efficiency during phase 2.7) except at the end of phase 2.3, as discussed above. Note that after phase 1.7 *p*-cresol loading rate was decreased to that of the phase 1.1, COD removal efficiency showed negative values (not shown in figure 4.1.5). This is because the HRT of the AnMBR was 4 days, meaning high concentration of *p*-cresol was still present in the reactor even a few days after the *p*-cresol loading rate was decreased to that of the phase 1.1. The calculation did not take into account the gradual decrease of *p*-cresol concentration inside the reactor in reality and thus resulted in negative values.

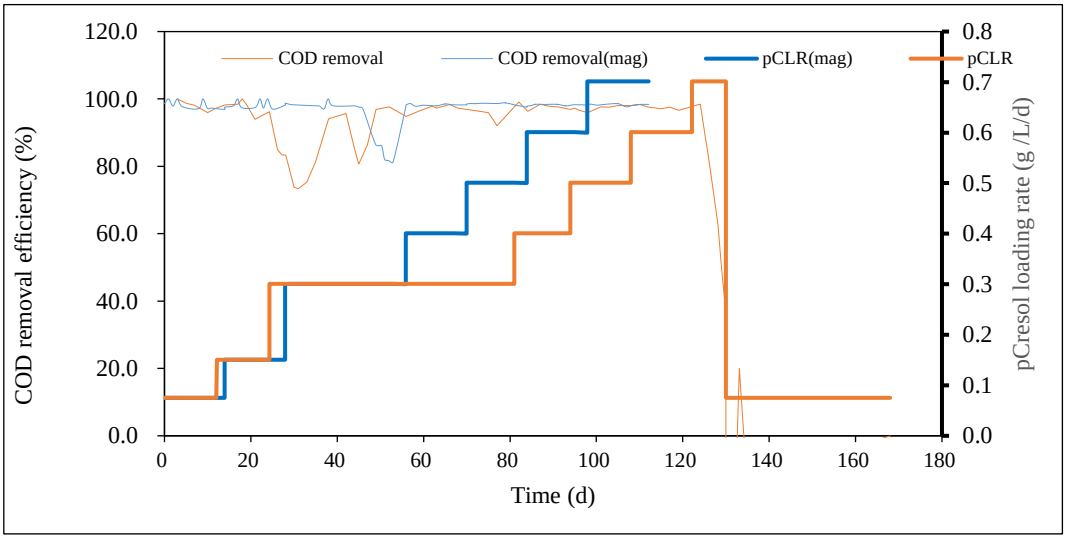

Figure 4.1.5 COD removal efficiency of the AnMBR during phase 1 without magnetite and phase 2 with magnetite

COD balance is shown in figure 4.1.6. When the reactor was stable, the COD balance of phase 1 remained approximately 75% in contrast to about 80% in phase 2. It did not reach 100% because part of COD was converted to biomass and this amount was not taken into consideration. COD balance also corresponds to the shock period during phase 1.3 (decrease of COD balance), reactor failure during phase 1.7 (specific methane production decreasing to 0) and stable reactor performance throughout phase 2 (stable specific methane production during phase 2.7) except at the end of phase 2.3, as discussed above. Stable COD balance within the reasonable range underpins the validity of the acquired experimental data.

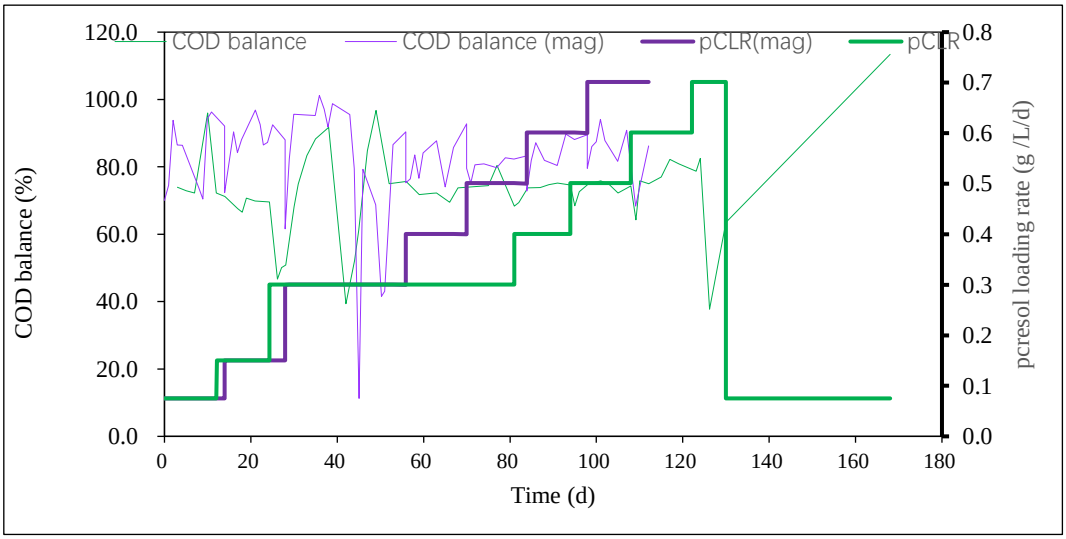

Figure 4.1.6 COD balance of the AnMBR during phase 1 without magnetite and phase 2 with magnetite

4.1.2. Increased dehydrogenase and coenzyme F_{420} activities possibly due to magnetite nanoparticles

More robust process stability induced by magnetite can be further illustrated by the increased dehydrogenase activities and F_{420} activities shown in figure 4.1.7. The activities of both enzymes remained higher in phase 2 than their counterparts in phase 1. Furthermore, enzyme activities during phase 2 did not decrease until phase 2.6. These observations indicate that such concentrations of *p*-cresol used in the experiments may have exerted a toxic effect on the microorganisms. Given that coenzyme F_{420} is associated with hydrogenotrophic methanogenic activity but not acetoclastic methanogenic activity (Dolfing & Mulder, 1985), the results imply that magnetite supplement may have improved hydrogenotrophic methanogenesis, and that magnetite supplement may have helped alleviate the toxic effect of *p*-cresol on methanogens.

Xu et al. (2020) studied the effect of activated carbon as well as goethite on methane production under acid stress. They found methane production under acid stress were improved by both activated carbon and goethite. Furthermore, F_{420} activities was significantly higher in groups with goethite addition in comparison with control groups while dehydrogenase activities were lower in groups with goethite than control groups. Xu et al. (2020) ascribed the enhanced F_{420} activities to iron increasing the concentration and activities of enzymes since iron is usually located in the key enzymatic center or coenzyme factor of methanogens. Decreased formate dehydrogenase activities indicate syntrophic partners shifts more to DIET path way (Xu et al., 2020). On the other hand, formate dehydrogenase activities were found to increase in the methanogenic system and genes encoding formate dehydrogenase were more abundant when magnetite was dosed (Yin et al., 2018a). But the genes were assigned to other microorganism, instead of methanogens. Therefore Yin et al. (2018)inferred formate dehydrogenase was involved in other pathways instead of methanogenesis.

In this research, higher enzymatic activities may have facilitated higher permissible OLR by increasing the stability of the reactor. However based on the discussion above, whether the increased dehydrogenase activities were ascribed to methanogens or other microorganisms needs further study.

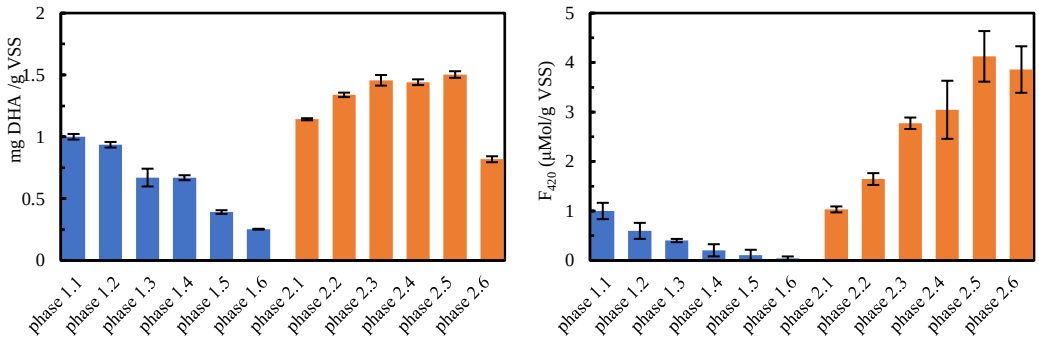

Figure 4.1.7 Both dehydrogenase activities (left) normalized to phase 1.1 and F_{420} activities (right) normalized to phase 1.1 increased possibly due to magnetite addition Phase 1 without magnetite; phase 2 with magnetite

4.1.3. Increased total microbial products due to increased *p*-cresol loading rate

Results of mixed liquor analysis are shown in figure 4.1.8 (total microbial products) and figure 4.1.9 (SMPs). In total microbial products, TOC in phase 2 was significantly higher, indicating magnetite stimulated the production of microbial products. But the SMPs in phase 2 remained similar to phase 1, indicating that increased TOC in phase 2 resulted from the increase of EPS. Higher concentration of EPS may protect the cells from toxic chemicals and reduce the toxicity, thus increasing process stability (Li et al., 2015). While polysaccharides concentration in phase 1 shows a decreasing trend, in phase 2 polysaccharides appear to be stable with increasing *p*-cresol loading rate. Proteins in both phases show an increasing trend, but the increment with magnetite addition is smaller than without magnetite. Humic like substances in both phases also show an increasing tendency. In SMPs, TOC, polysaccharides and humic like substances show the trend as those in total microbial products discussed above. But proteins in SMPs in phase 2 show an decreasing trend, contrary to that of proteins in total microbial products.

Zhou et al. (2020) reported that magnetite reduced the SMPs (magnetite group 9.79 ± 1.34 mg/L in comparison with 15.31 ± 0.53 mg/L) as well as EPS concentration in an aerobic MBR by means of enhancing dehydrogenase activities and therefore accelerating the degradation of SMPs and EPS. Other researchers claimed that addition of magnetite, despite enhanced COD removal and methane productivity, increased

SMPs concentration due to increased concentration of Fe^{2+} from corrosion of magnetite nano particles (Zhong et al., 2020). Increased F_{420} activities may have also benefited from this, as discussed in section 4.1.2. The SMPs concentration in this study remained similar. Based on the results of other studies mentioned above, this may be caused by the comprehensive effect of increased enzyme activities boosting degradation of SMPs and corrosion of magnetite enhancing production of SMPs. Further study needs to investigate the effect of magnetite corrosion on mixed liquor properties in order to obtain conclusive evidence.

Change of median particle size over *p*-cresol loading rate in figure 4.1.10 shows that with increasing *p*-cresol loading rate, the median particle size became smaller, rendering the AnMBR more prone to fouling. In phase 2 with magnetite, the reduction of median particle size is more evenly distributed over the increase of *p*-cresol loading rate compared to in phase 1.

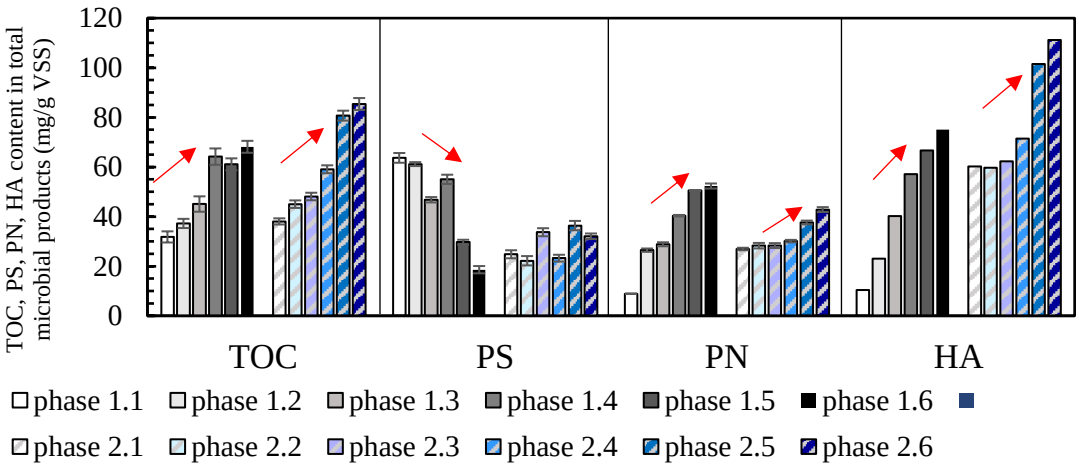

* All tendencies marked by red arrows are statistically significant (Spearman correlation between *p*-cresol loading rate and TOC, PS, PN, HA) with $p<0.01$

Figure 4.1.8 Composition of total microbial products of mixed liquor, where TOC – total organic carbon, PS – polysaccharide, PN – protein, HA – humic like substances

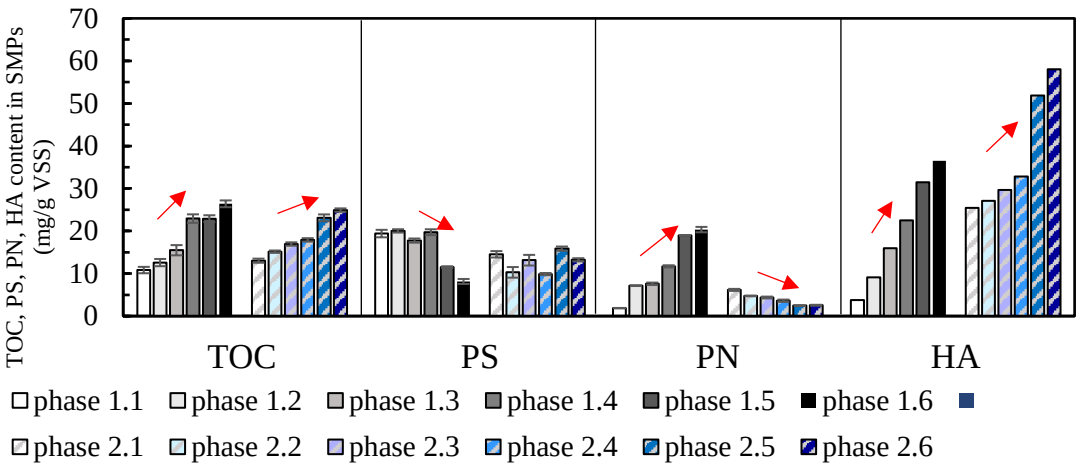

* All tendencies marked by red arrows are statistically significant (Spearman correlation between *p*-cresol loading rate and TOC, PS, PN, HA) with $p<0.05$

Figure 4.1.9 Composition of SMPs of mixed liquor where TOC – total organic carbon, PS – polysaccharide, PN – protein, HA – humic like substances

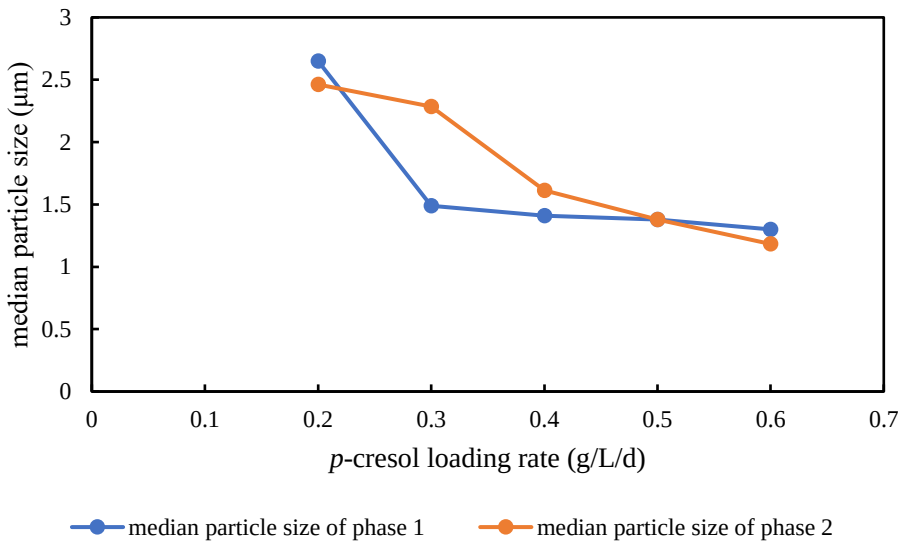

Figure 4.1.10 Median particle size versus p-cresol loading rate in phase 1 without magnetite and phase 2 with magnetite

4.1.4. Increased fouling potential with increasing *p*-cresol loading rate correlated with increasing protein concentration

Figure 4.1.11 shows the fouling potential of the supernatant of the reactor mixed liquor. For both phases, the fouling potential of the supernatant increased with the increasing *p*-cresol loading rate. Furthermore, fouling potential under the same *p*-cresol loading rates in phase 2 is smaller than that of phase 1, indicating magnetite supplementation reduced the fouling potential of the supernatant of the mixed liquor. It should be noticed that magnetite nanoparticles could act as a foulant themselves. Further research should investigate the fouling potential of the mixed liquor.

Correlation analysis is shown in figure 4.1.12 The first row of figure 4.1.12 indicates that the increasing fouling potential with the increasing *p*-cresol loading rate in phase 1 was correlated with the increase of both proteins and humic like substances, whereas the second row explains the increasing fouling potential with the increasing *p*-cresol loading rate in phase 2 was correlated with the increase of humic like substances. The first and second row combined indicate the fouling potential was not contributed by increase of polysaccharides in SMPs. The third row implies that proteins had a bigger impact on the fouling potential in both phase 1 and phase 2, and thus in phase 2 the fouling potential was smaller likely due to less proteins in SMPs.

Decreased fouling potential was also observed in an aerobic MBR supplemented with magnetite nano particles (Zhou et al., 2020), which can be attributed to faster degradation of EPS and SMPs by enhanced enzyme activities due to magnetite.

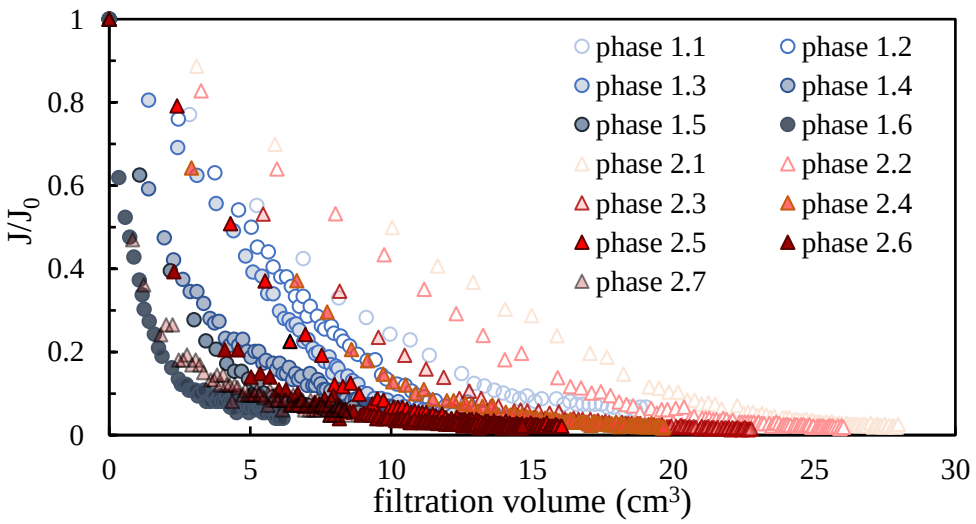

Figure 4.1.11 Fouling potential of the supernatant of the reactor mixed liquor. Real-time flux J normalized to the initial flux J_0

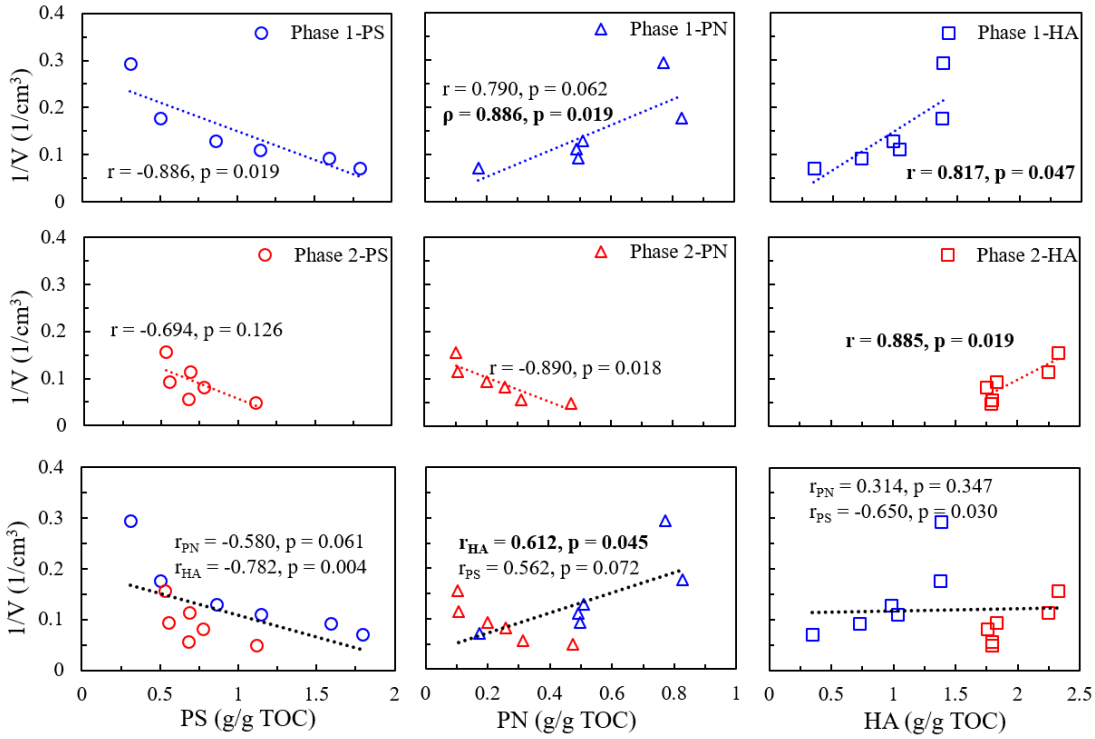

Figure 4.1.12 Correlation between PS, PN, HA in SMPs and fouling potential.
1/V: V represents the volume when J/J_0 equals 0.1
r: Pearson's correlation coefficient
ρ: Spearman's rank correlation coefficient, p: two-tailed test value

Results of section 4.1 have the following implications. First, the application of magnetite to anaerobic digestion may reduce the size of the reactor as well as the energy consumption and the operational costs by increasing the maximal OLR and increasing the flux / reducing the maintenance fees of membrane. Second, magnetite may significantly change the composition of the microbial community, resulting in more bacteria and methanogens capable of DIET (Lei et al., 2018) and consequent higher degrading ability and higher permissible OLR. Meanwhile magnetite may also induce hydrogenotrophic methanogenic pathway, consistent with the findings of Yin et al. (2018b). Third, shifted microbial community tended to secrete more EPS instead of SMP. More EPS act as a protective layer for microbial cells (Yan et al., 2018) and thus may have led to enhanced reactor stability and resistance. At the same time the shifted microbial community tended not to secrete SMP associated with high fouling potential, implying magnetite may reduce the fouling potential of the supernatant of the mixed liquor.

4.2. Batch experiments about *p*-cresol degradation pathway

4.2.1. Substrate degradation inhibited by BES but accelerated by magnetite

Substrate degradation of control group batch experiment 1 is shown in figure 4.2.1. Results of batch experiment 2 are shown in figure 4.2 in appendix. Because some groups of *p*-cresol and benzoate degradation in batch experiment 2 had not yet initiated by the end of the experiment, it was not possible to obtain sufficient data to comprehensively discuss substrate degradation using the experimental data from batch experiment 2. Therefore the substrate degradation to be discussed below is based on the results of batch experiment 1.

Conversion of *p*-cresol, benzoate and propionate was significantly accelerated in the magnetite groups compared to the control group, as is illustrated by the modeled maximum substrate degradation rate (denoted as R_m) shown in table 4.1 and table 4.2. While R_m of *p*-cresol, benzoate and propionate were all improved by magnetite addition, R_m of benzoate was enhanced to the largest degree. Given that benzoate is a central compound of methanogenic degradation of many aromatic compounds (Dangel et al., 1991; Heider & Fuchs, 1997), magnetite may also enhance the methanogenic degradation of other aromatic compounds.

BES addition led to accumulation of VFAs. At the same time, accumulation of VFAs inhibits the degradation of *p*-cresol and benzoate. By comparing BES and BES+magnetite groups of *p*-cresol and benzoate (see figure 4.2.1 A and C), it can be concluded that magnetite did not only accelerate the conversion of VFAs, but also the conversion from benzoate to VFAs. This acceleration was especially obvious in the BES+magnetite group compared to BES group of benzoate because the VFAs accumulation in BES+magnetite group was considerably higher than BES group of benzoate.

4HBA in all groups was degraded rapidly to phenol. Magnetite accelerated the conversion of 4HBA while BES improved its conversion even more than magnetite (control: Rm= 149.6, BES: Rm=426.9, Mag: Rm= 246.0, BES+Mag: Rm= 417.0, the unit is $mg \cdot L^{-1} \cdot d^{-1}$). This indicates conversion of 4HBA was not thermodynamically inhibited by the accumulation of phenol.

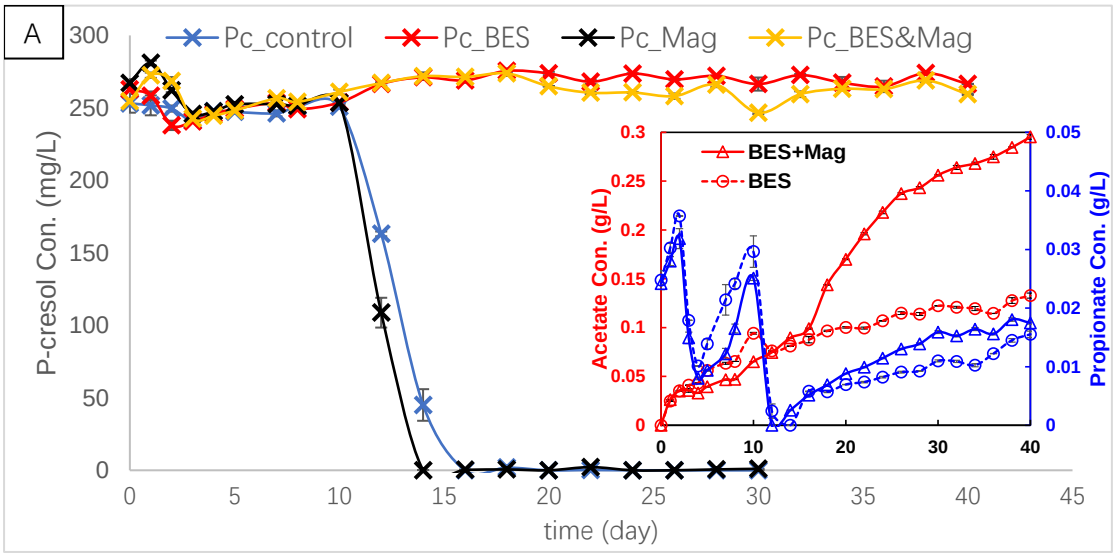
A
Pc_control
Pc_BES
Pc_Mag
Pc_BES&Mag
P-cresol Con. (mg/L)
time (day)
BES+Mag
BES
Acetate Con. (g/L)
Propionate Con. (g/L)

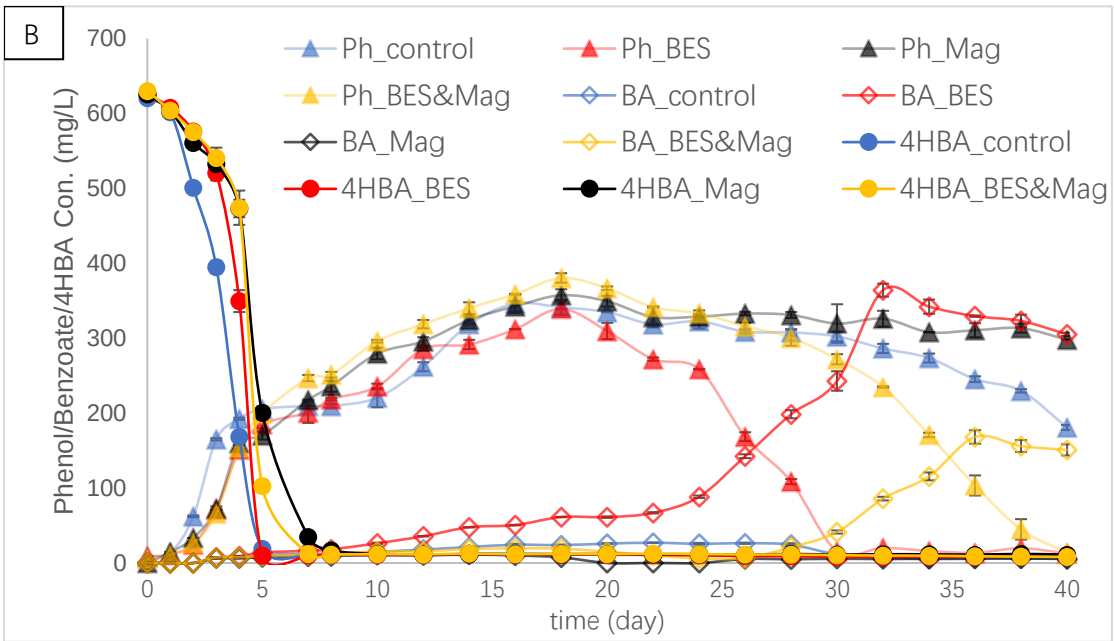
B
Ph_control
Ph_BES
Ph_Mag
Ph_BES&Mag
BA_control
BA_BES
BA_Mag
BA_BES&Mag
4HBA_control
4HBA_BES
4HBA_Mag
4HBA_BES&Mag
Phenol/Benzoate/4HBA Con. (mg/L)
time (day)

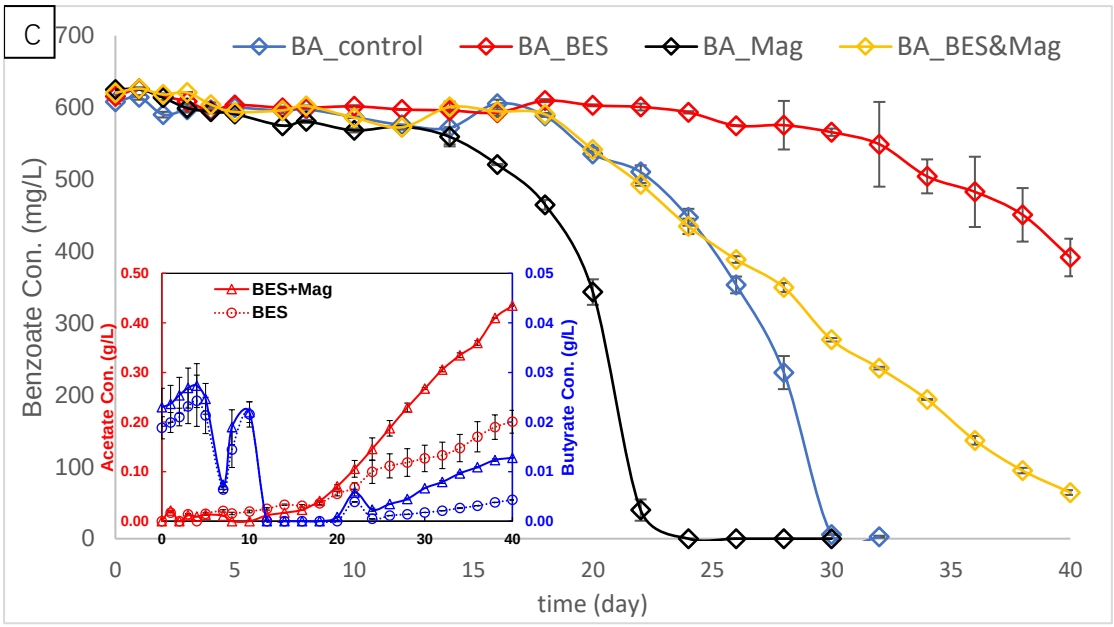

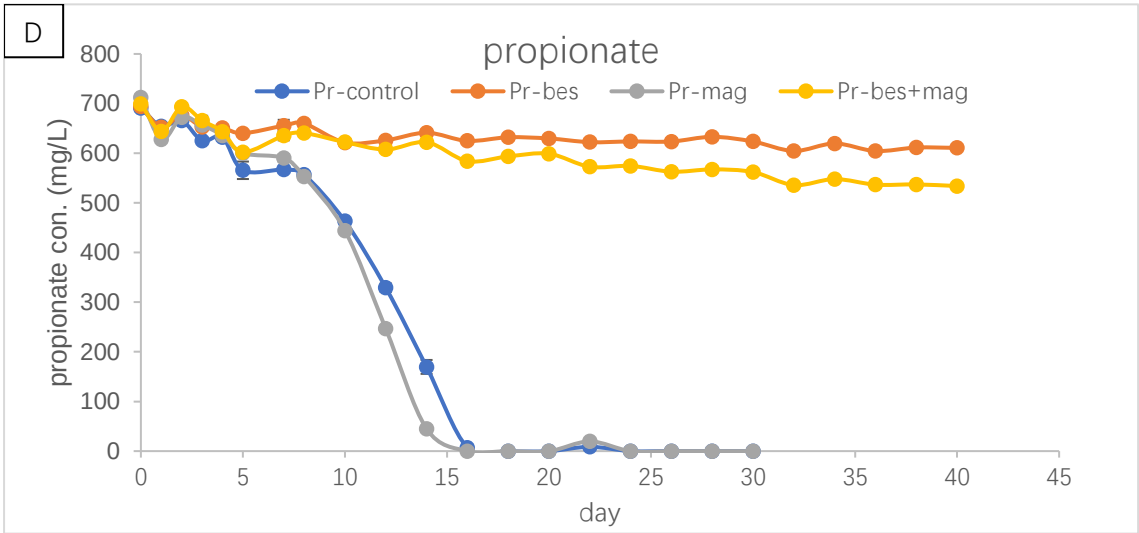

Figure 4.2.1 Substrate degradation in batch experiment 1

Pc: *p*-cresol

4HBA: 4-hydroxybenzoate

BA: benzoate

Pr: propionate

4.2.2. Accumulative methane production inhibited by BES but accelerated by magnetite

For *p*-cresol, benzoate and propionate, accumulative methane production within same time in groups with only magnetite addition was significantly higher than that in control group, indicating magnetite can accelerate the metabolism of the substrates, which is in accordance with the enhanced maximum substrate degradation rate. In some cases, e.g. control and magnetite groups of propionate shown in figure 4.2.2, accumulative methane production exceeded theoretical methane production. However, substrate and its intermediate had already been depleted by day 18, as can be seen in figure 4.2.1 D. Therefore, methane production after day 18 in those groups did not result from degradation of the substrate. Instead, microorganisms may have used other substances, e.g. cell debris, EPS, for methane production. Groups with BES addition had very little degradation of substrates as well as methane production, except that benzoate could still be converted to acetate (see figure 4.1 and figure 4.2 in appendix) in the groups with BES but methanogenesis was still impeded.

Furthermore, total methane production in the magnetite groups was higher than that in the control groups when substrates were depleted. This indicated magnetite might have also boosted catabolism. However, this has not yet been reported by previous studies on DIET.

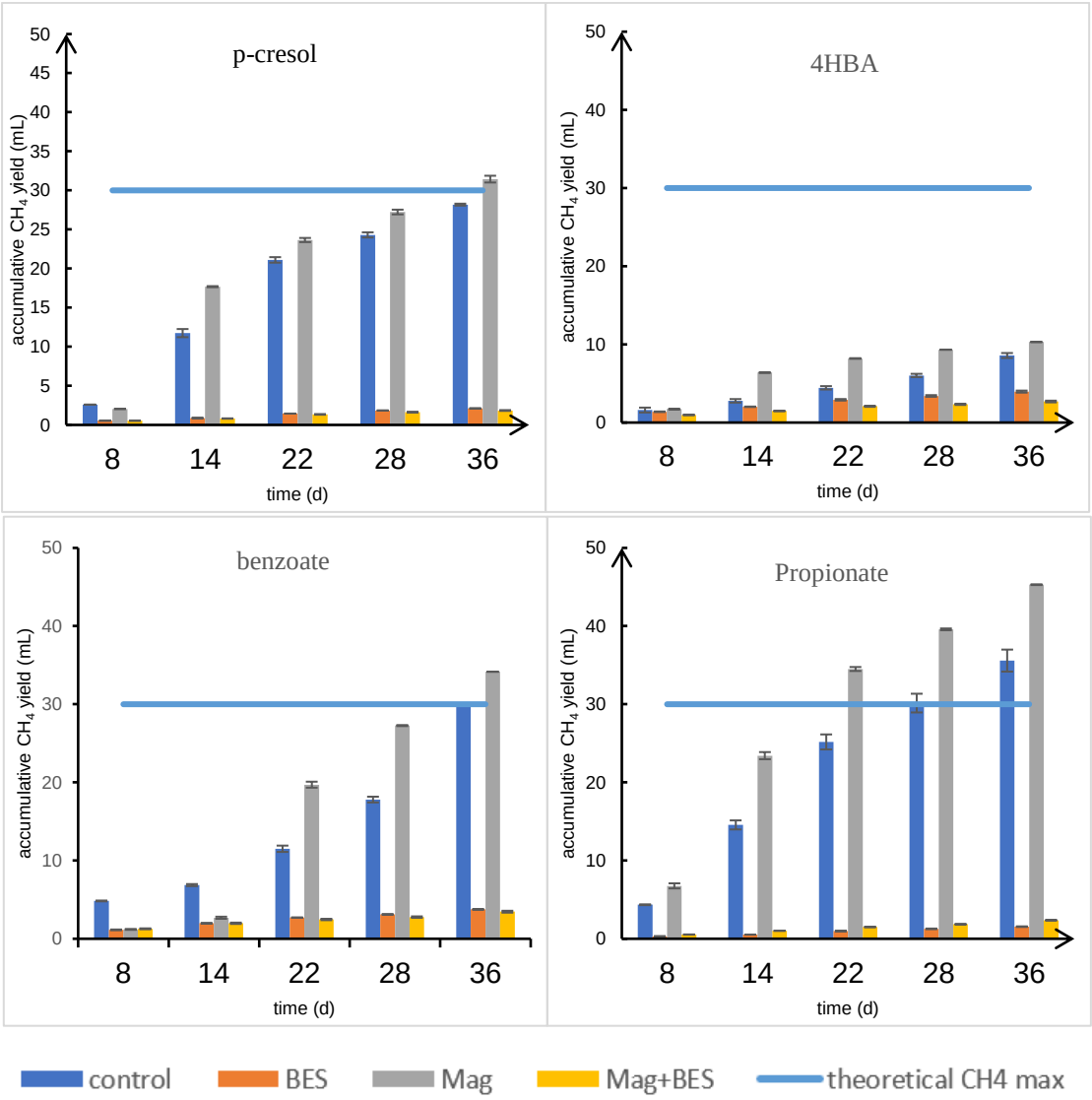

Figure 4.2.2 Accumulative methane yield in batch experiment 1

4.2.3. Conversion of benzoate as the rate limiting step

Rate limiting step is derived from the control groups in batch experiment 1. As shown in figure 4.2.3, for *p*-cresol and benzoate, no aromatic compounds were detected and VFAs did not accumulate. For 4HBA, it was rapidly converted to phenol. Phenol accumulated while benzoate did not, indicating benzoate was quickly degraded. During the degradation of 4HBA, methane was detected since the beginning of the batch experiment 1, shown in 4.2.2 , meaning certain amount of 4HBA was completely reduced to methane. If the initial concentration of 4HBA was low, phenol accumulation might have not occurred, as was in the case of *p*-cresol degradation, implying 4HBA

would not accumulate during the degradation of *p*-cresol. Therefore, phenol accumulation is not taken into account for *p*-cresol degradation.

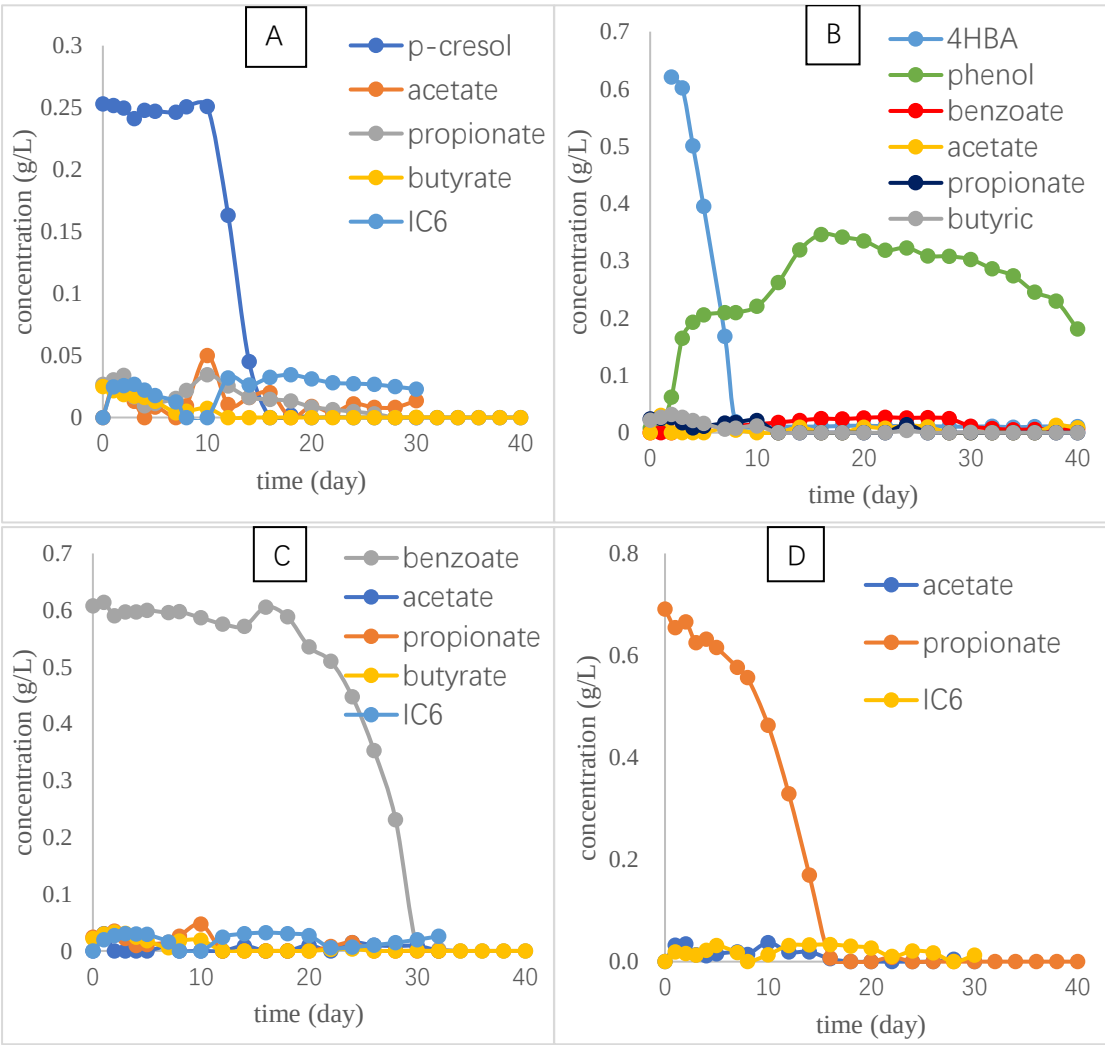

Figure 4.2.3 Substrate degradation of control groups with substrate and their intermediates in batch experiment 1

A. substrate: *p*-cresol; B. substrate: 4HBA;

C. substrate: benzoate; D. substrate: propionate

Modeled results are shown in table 4.1 and table 4.2. Gompertz and Logistic model both fitted the experimental data well as evidenced by the reasonably high Pearson's correlation coefficient. But because the Pearson's correlation coefficients of the Logistic model are in general slightly higher, the maximum substrate degradation rate (denoted as Rm) and lag phase (denoted as λ) discussed below are based on the results of the Logistic model.

In all control groups of batch experiment 1, Rm (4HBA > propionate >p-cresol > benzoate), shown in figure 4.2.4. It can be concluded that the rate limiting step of methanogenic conversion of *p*-cresol without enhancement of DIET was the conversion of benzoate.

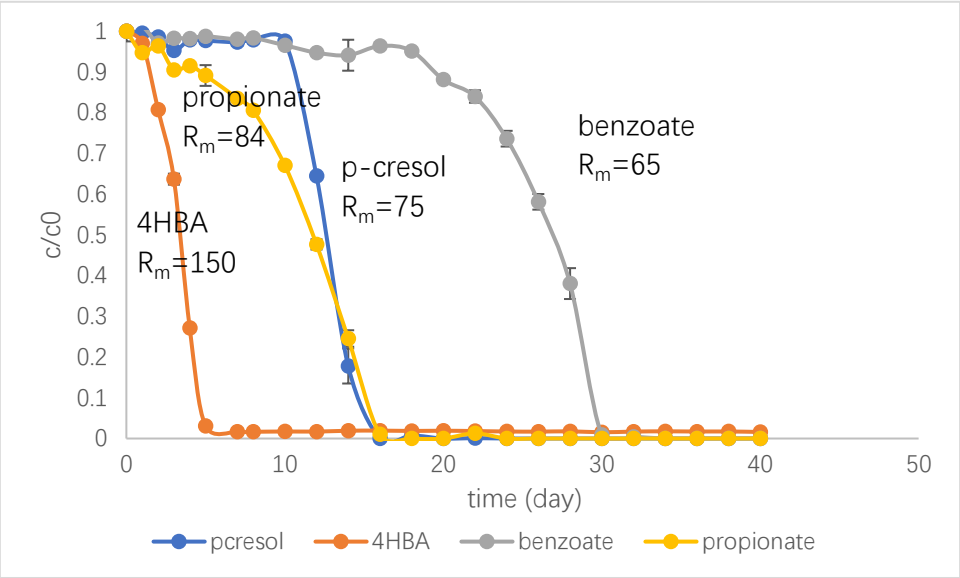

Figure 4.2.4 Comparison of substrate degradation rate. Concentration is normalized to the initial concentration. The unit of R_m is $mg \cdot L^{-1} \cdot d^{-1}$

Table 4. 1 Modeled parameters of Gompertz and Logistic model of batch experiment 1

		Gompertz				Logisctic				
		Rm(mg/L/d)	λ(d)	coefficient	p-value	Rm(mg/L/d)	λ(d)	coefficient	p-value	coefficient Gompertz - coefficient Logistic
pcresol	control	80	11	9.989×10^{-01}	$8.9.\times10^{-31}$	75	11	9.986×10^{-01}	1.4×10^{-29}	3.13×10^{-04}
	BES	\	\	\	\	\	\	\	\	
	Mag	795	12	9.986×10^{-01}	$1.4.\times10^{-29}$	152	11	9.986×10^{-01}	1.3×10^{-29}	-1.35×10^{-05}
	BES Mag	\	\	\	\	\	\	\	\	
4HBA	control	222	2	9.960×10^{-01}	$1.5.\times10^{-24}$	150	2	9.983×10^{-01}	1.2×10^{-28}	-2.31×10^{-03}
	BES	847	4	9.972×10^{-01}	$3.3.\times10^{-26}$	427	3	9.976×10^{-01}	4.6×10^{-27}	-4.62×10^{-04}
	Mag	269	4	9.977×10^{-01}	$3.3.\times10^{-27}$	246	3	9.984×10^{-01}	6.4×10^{-29}	-6.92×10^{-04}
	BES Mag	463	4	9.981×10^{-01}	$3.4.\times10^{-28}$	417	4	9.984×10^{-01}	5.9×10^{-29}	-2.79×10^{-04}
benzoate	control	69	23	9.927×10^{-01}	$1.0.\times10^{-21}$	65	23	9.957×10^{-01}	3.1×10^{-24}	-2.99×10^{-03}
	BES	16	30	9.884×10^{-01}	$1.7.\times10^{-19}$	24	33	9.904×10^{-01}	2.0×10^{-20}	-2.07×10^{-03}
	Mag	108	18	9.943×10^{-01}	$7.0.\times10^{-23}$	105	18	9.964×10-01	4.9×10^{-25}	-2.07×10^{-03}
	BES Mag	25	19	9.971×10^{-01}	$3.7.\times10^{-26}$	25	19	9.971×10^{-01}	4.1×10^{-26}	2.64×10^{-05}
propionate	control	91	8	9.944×10^{-01}	$5.5.\times10^{-23}$	84	8	9.969×10^{-01}	9.9×10^{-26}	-2.44×10^{-03}
	BES	\	\	\	\	\	\	\	\	\

	Mag	112	8	9.956×10^{-01}	$3.6.\times10^{-24}$	106	8	9.976×10^{-01}	5.7×10^{-27}	-1.93×10^{-03}
	BES Mag	\	\	\	\	\	\	\	\	\

Table 4. 2 Modeled parameters of Gompertz and Logistic model of batch experiment 2

		Gompertz				Logisctics				
		Rm(mg/L/d)	λ(d)	coefficient	p-value	Rm(mg/L/d)	λ(d)	coefficient	p-value	coefficient Gompertz - coefficient Logistic
pcresol	control	\	\	\	\	\	\	\	\	\
	BES	\	\	\	\	\	\	\	\	\
	Mag	43	37	9.923×10^{-01}	1.1×10^{-18}	43	37	9.952×10^{-01}	1.1×10^{-20}	-2.97×10^{-03}
	BES Mag	\	\	\	\	\	\	\	\	\
4HBA	control	367	2	9.992×10^{-01}	6.5×10^{-31}	378	2	9.999×10^{-01}	1.9×10^{-42}	-7.26×10^{-04}
	BES	341	3	9.989×10^{-01}	2.0×10^{-29}	321	3	9.995×10^{-01}	2.2×10^{-33}	-6.34×10^{-04}
	Mag	321	2	9.994×10^{-01}	2.4×10^{-32}	293	2	9.999×10^{-01}	6.9×10^{-40}	-4.66×10^{-04}

	BES Mag	332	3	9.983×10^{-01}	2.7×10^{-27}	296	3	9.997×10^{-01}	3.6×10^{-35}	-1.44×10^{-03}
benzoate	control	51	32	9.781×10^{-01}	4.2×10^{-15}	51	32	9.867×10^{-01}	2.9×10^{-17}	-8.63×10^{-03}
	BES	0	31	9.440×10^{-01}	4.4×10^{-11}	0	36	8.982×10^{-01}	1.4×10^{-08}	4.58×10^{-02}
	Mag	81	29	9.922×10^{-01}	1.4×10^{-19}	79	29	9.955×10^{-01}	5.8×10^{-22}	-3.31×10^{-03}
	BES Mag	0	28	9.718×10^{-01}	5.1×10^{-14}	0	32	9.601×10^{-01}	1.6×10^{-12}	1.17×10^{-02}
propionate	control	76	15	9.935×10^{-01}	2.3×10^{-20}	72	15	9.955×10^{-01}	6.7×10^{-22}	-1.94×10^{-03}
	BES	3	32	6.236×10^{-01}	1.9×10^{-03}	6	45	6.236×10^{-01}	1.9×10^{-03}	-5.96×10^{-05}
	Mag	79	12	9.946×10^{-01}	3.9×10^{-21}	74	12	9.969×10^{-01}	1.3×10^{-23}	-2.35×10^{-03}
	BES Mag	\	\	\	\	\	\	\	\	\

4.2.4. Potential loss of microorganisms possibly due to aggregation between magnetite nanoparticles and microorganisms

Despite that batch experiment 2 yielded the same rate limiting step (see table 4.2) and similar tendencies of substrate degradation (see figure 4.2 in appendix), it had been expected that batch experiment 2 should have resulted in higher R_m and λ because the inoculum had already been adapted to magnetite. However this was not the case. Both R_m and λ of *p*-cresol, benzoate and propionate of control groups were higher in batch experiment 1 rather than in batch experiment 2. Meanwhile the R_m of 4HBA was bigger. A plausible explanation is that since magnetite has been found to closely associated with the DIET microbial aggregates (Cruz Viggi et al., 2014), loss of DIET-based biomass may have occurred due to insufficient shaking when magnetite was taken out from the inoculum collected during phase 2.3. Therefore the abundance of DIET-based microorganisms may have been reduced while non DIET-based biomass may have been enriched in the inoculum of batch experiment 1. This hypothesis can be tested by investigating the microbial community of the inoculum of batch experiment 1 and batch experiment 2.

Potential loss of biomass implies that research on how to cost-effectively separate biomass and magnetite nanoparticles may be important for application of magnetite in lab-scale reactor or even full-scale reactor to prevent the decrease of treating capacity.

On the other hand, despite the likely loss of biomass in the beginning of batch experiment 2, R_m of 4HBA of the control group of batch experiment 2 is much bigger than that of the batch experiment 1, implying the 4HBA degrading bacteria may have not aggregated with magnetite and conversion of 4HBA may not depend on the DIET-based microorganisms.

4.3. 20 mmol / g VSS as optimal magnetite nanoparticles dosage

The results of optimization of magnetite dosage using *p*-cresol as starting substrate is shown in figure 4.3.1. It was not possible to calculate cumulative methane production because gas composition data were distorted. Compared to control group, substrate degradation in groups of 10 mmol/L and 20 mmol/L was accelerated, with 20 mmol/L being the optimal dosage. 30 mmol/L resulted in the similar degradation rate compared to the control group. Groups with 40 mmol/L and higher magnetite addition hampered the degradation and complete halt of degradation was achieved by 75 mmol/L and higher magnetite dosage. This may be due to the toxic effect of released ions of higher dosage (Noonari et al., 2019). Results of abiotic loss shown in figure 4.3.2 indicate magnetite nanoparticles up to 200 mmol/L did not cause any adsorption.

Since starting VSS concentration was 1 g/L, the optimal dosage of magnetite was 20 mmol / g VSS. The VSS concentration in both phases in the AnMBR was above 4 g/L, meaning the magnetite dosage in the AnMBR did not reach the optimum.

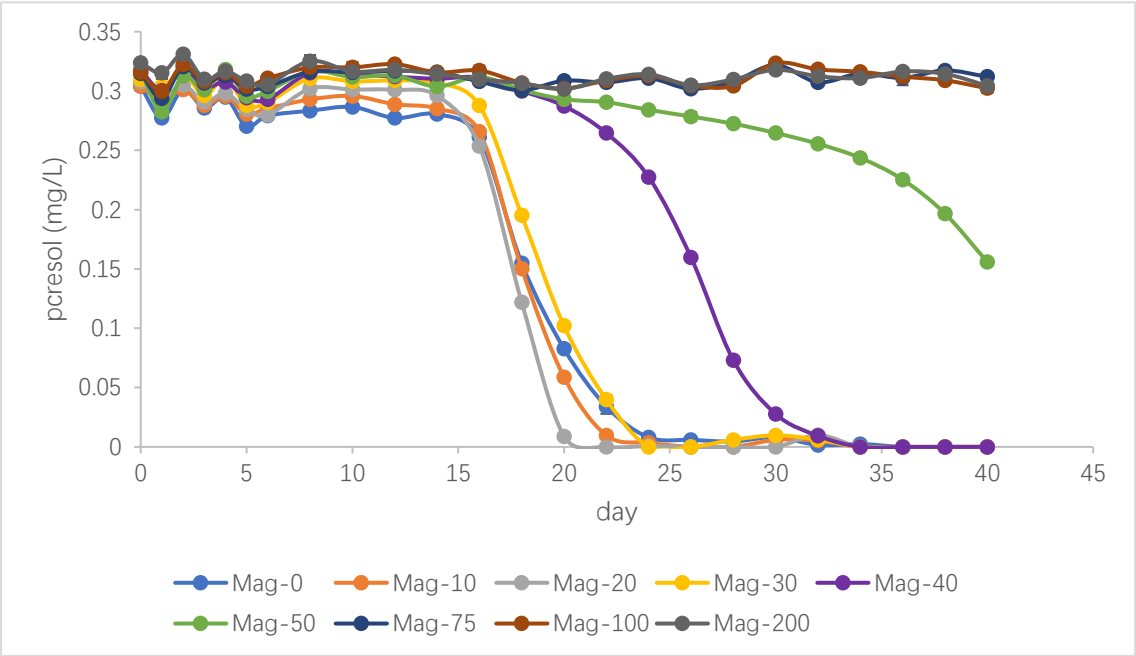

Figure 4.3.1 degradation of *p*-cresol under different concentration of magnetite

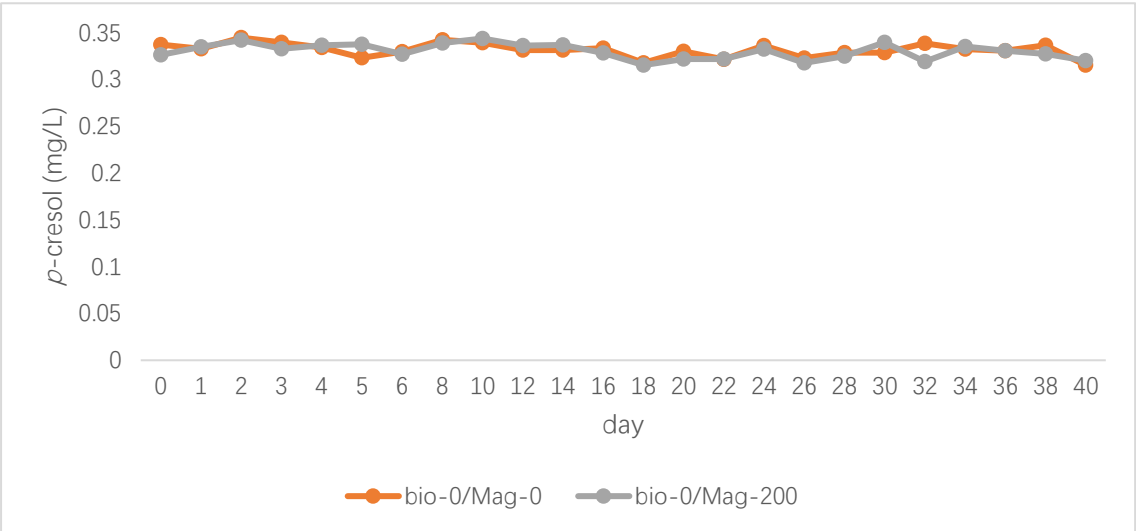

Figure 4.3.2 Abiotic effect of magnetite on substrate degradation

5. Conclusions and recommendations

This research studied the effect of magnetite on the methanogenic degradation of *p*-cresol in an AnMBR. Magnetite permitted higher maximal *p*-cresol loading rate of the AnMBR, rendered the reactor more resistant to toxicity and resulted in lower fouling potential of the supernatant of the mixed liquor. COD removal efficiency and methane production rate remained similar in the AnMBR when supplemented with magnetite compared with the stage without magnetite supplement. Activities of dehydrogenase and F_{420} was significantly enhanced. Due to the aforementioned results, potential commercial application of magnetite nanoparticles in AnMBR may permit shorter hydraulic retention time (HRT) and higher flux, which can lead to higher treatment capacity and lower operational costs. Furthermore, it was found that magnetite could accelerate the degradation of all intermediates chosen in this research and that the rate limiting step of methanogenic conversion of *p*-cresol is the conversion of benzoate, which magnetite could significantly improve. The optimal dosage of magnetite was 20 mmol / g VSS.

Based on the discussions in chapter 4, two recommendations for further research are proposed:

1. Because the corrosion of magnetite may occur and released Fe^{2+} can increase the SMP concentration and high concentration of Fe^{2+} may be toxic to microorganisms (Noonari et al., 2019; Zhong et al., 2020), it is hypothesized that magnetite concentration in the reactor will decrease over time and increasing SMP concentration due to increased Fe^{2+} concentration may increase fouling potential of the supernatant in the long run. It is therefore recommended to investigate the long-term effect of magnetite corrosion on the mixed liquor properties, fouling potential and the composition of microbial community.
2. Because magnetite has been found to closely associated with the DIET microbial aggregates (Cruz Viggi et al., 2014), it is hypothesized that loss of biomass may occur if the magnetite nanoparticles are to be removed from the reactor. Consequently treating capacity of the reactor will decrease. It is therefore recommended to investigate the effect of magnetite removal on the composition of microbial community and methods to remove magnetite nanoparticles with as little loss of biomass as possible.

References

Anderson, A. (2006). Final report on the safety assessment of sodium p-Chloro-m-Cresol, p-Chloro-m-Cresol, Chlorothymol, Mixed Cresols, m-Cresol, o-Cresol, p-Cresol, Isopropyl Cresols, Thymol, o-Cymen-5-ol, and Carvacrol. *International Journal of Toxicology*, *25*(Supplement. 1), 29–127.

Baek, G., Jung, H., Kim, J., & Lee, C. (2017). A long-term study on the effect of magnetite supplementation in continuous anaerobic digestion of dairy effluent – Magnetic separation and recycling of magnetite. *Bioresource Technology*, *241*, 830–840.

Barua, S., & Dhar, B. R. (2017). Advances towards understanding and engineering direct interspecies electron transfer in anaerobic digestion. *Bioresource Technology*, *244*, 698–707.

Cheng, Q., & Call, D. F. (2016). Hardwiring microbes: Via direct interspecies electron transfer: Mechanisms and applications. *Environmental Science: Processes and Impacts*, *18*(8), 968–980.

Collins, G., Foy, C., McHugh, S., Mahony, T., & O'Flaherty, V. (2005). Anaerobic biological treatment of phenolic wastewater at 15-18°C. *Water Research*, *39*(8), 1614–1620.

Cruz Viggi, C., Rossetti, S., Fazi, S., Paiano, P., Majone, M., & Aulenta, F. (2014). Magnetite particles triggering a faster and more robust syntrophic pathway of methanogenic propionate degradation. *Environmental Science and Technology*, *48*(13), 7536–7543.

Dang, Y., Holmes, D. E., Zhao, Z., Woodard, T. L., Zhang, Y., Sun, D., Wang, L. Y., Nevin, K. P., & Lovley, D. R. (2016). Enhancing anaerobic digestion of complex organic waste with carbon-based conductive materials. *Bioresource Technology*, *220*, 516–522.

Dangel, W., Brackmann, R., Lack, A., Mohamed, M., Koch, J., Oswald, B., Seyfried, B., Tschech, A., & Fuchs, G. (1991). *Hicrnbiology*. *l 991*, 256–262.

Dolfing, J., & Mulder, J.-W. (1985). Comparison of Methane Production Rate and Coenzyme F420 Content of Methanogenic Consortia in Anaerobic Granular Sludget. *Applied and Environmental Microbiology*, *49*(5), 1142-1145.

Dubois, M., Gilles, K. A., Hamilton, J. K., Rebers, P. A., & Smith, F. (n.d.). Colorimetric Method for Determination of Sugars and Related Substances. *Analytical Chemistry*, *28*, 350-356

Dvořák, L., Gómez, M., Dolina, J., & Černín, A. (2016). Anaerobic membrane bioreactors—a mini review with emphasis on industrial wastewater treatment: applications, limitations and perspectives. *Desalination and Water Treatment*, *57*(41), 19062–19076.

Energie en waterbeheer. Bouwstenen voor de energietransitie | STOWA. (n.d.). Retrieved July 21, 2020, from https://www.stowa.nl/publicaties/energie-en-waterbeheer-bouwstenen-voor-de-energietransitie

Frølund, B., Griebe, • T, & Nielsen, P. H. (1995). Enzymatic activity in the activated-sludge floc matrix. *Applied Microbiol Biotechnology, 43*, 755-761

Gujer, W., & Zehnder, A. J. B. (1983). Conversion processes in anaerobic digestion. *Water Science and Technology*, *15*(8–9), 127–167.

Häggblom, M. M., Rivera, M. D., Bossert, I. D., Rogers, J. E., & Young, L. Y. (1990). Anaerobic biodegradation of Para-cresol under three reducing conditions. *Microbial Ecology*, *20*(1), 141–150.

Heider, J., & Fuchs, G. (1997). Anaerobic metabolism of aromatic compounds. *European Journal of Biochemistry*, *243*(3), 577–596.

Jalayeri, H., Doulati Ardejani, F., Marandi, R., & Rafiee pur, S. (2013). Biodegradation of phenol from a synthetic aqueous system using acclimatized activated sludge. *Arabian Journal of Geosciences*, *6*(10), 3847-3852

Kato, S., Hashimoto, K., & Watanabe, K. (2012). Methanogenesis facilitated by electric syntrophy via (semi)conductive iron-oxide minerals. *Environmental Microbiology*, *14*(7), 1646–1654.

Kreuk, M. De. (2018). *CIE4703 Wastewater Treatment*. *December*.

Lee, J., Koo, T., Yulisa, A., & Hwang, S. (2019). Magnetite as an enhancer in methanogenic degradation of volatile fatty acids under ammonia-stressed condition. *Journal of Environmental Management*, *241*, 418–426.

Lei, Y., Sun, D., Dang, Y., Chen, H., Zhao, Z., Zhang, Y., & Holmes, D. E. (2016). Stimulation of methanogenesis in anaerobic digesters treating leachate from a municipal solid waste incineration plant with carbon cloth. *Bioresource Technology*, *222*, 270–276.

Lei, Y., Wei, L., Liu, T., Xiao, Y., Dang, Y., Sun, D., & Holmes, D. E. (2018). Magnetite enhances anaerobic digestion and methanogenesis of fresh leachate from a municipal solid waste incineration plant. *Chemical Engineering Journal*, *348*, 992–999.

Li, J., Gu, J. D., & Pan, L. (2005). Transformation of dimethyl phthalate, dimethyl isophthalate and dimethyl terephthalate by Rhodococcus rubber Sa and modeling the processes using the modified Gompertz model. *International Biodeterioration and Biodegradation*, *55*(3), 223–232.

Li, L. L., Tong, Z. H., Fang, C. Y., Chu, J., & Yu, H. Q. (2015). Response of anaerobic granular sludge to single-wall carbon nanotube exposure. *Water Research*, *70*, 1–8.

Lin, H., Gao, W., Meng, F., Liao, B.-Q., Leung, K.-T., Zhao, L., Chen, J., & Hong, H. (2012). Membrane Bioreactors for Industrial Wastewater Treatment: A Critical Review. *Critical Reviews in Environmental Science and Technology*, *42*(7), 677–740.

Lin, H., Peng, W., Zhang, M., Chen, J., Hong, H., & Zhang, Y. (2013). A review on anaerobic membrane bioreactors: Applications, membrane fouling and future perspectives. *Desalination*, *314*, 169–188.

Liu, F., Rotaru, A. E., Shrestha, P. M., Malvankar, N. S., Nevin, K. P., & Lovley, D. R. (2012). Promoting direct interspecies electron transfer with activated carbon. *Energy and Environmental Science*, *5*(10), 8982–8989.

Liu, F., Rotaru, A. E., Shrestha, P. M., Malvankar, N. S., Nevin, K. P., & Lovley, D. R. (2015). Magnetite compensates for the lack of a pilin-associated c-type cytochrome in extracellular electron exchange. *Environmental Microbiology*, *17*(3), 648–655.

Lovley, D. R. (2011). Live wires: Direct extracellular electron exchange for bioenergy and the bioremediation of energy-related contamination. *Energy and Environmental Science*, *4*(12), 4896–4906.

Lovley, D. R. (2017a). Syntrophy Goes Electric: Direct Interspecies Electron Transfer. *Annual Review of Microbiolog*, *71*, 643-664

Lovley, D. R. (2017b). Happy together: Microbial communities that hook up to swap electrons. *ISME Journal 11*(2), 327–336).

Morgan, J. W., Forster, C. F., & Evison, L. (1990). A comparative study of the nature of biopolymers extracted from anaerobic and activated sludges. *Water Research*, *24*(6), 743–750.

Morita, M., Malvankar, N., Franks, A., Summers, Z., Giloteaux, L., Rotaru, A., Rotaru, C., & Lovley, D. (2011). Potential for Direct Interspecies Electron Transfer in Methanogenic. *Mbio*, *2*(4), 5–7.

Muñoz Sierra, Julian D., Oosterkamp, M. J., Wang, W., Spanjers, H., & van Lier, J. B. (2018). Impact of long-term salinity exposure in anaerobic membrane bioreactors treating phenolic wastewater: Performance robustness and endured microbial community. *Water Research*, *141*, 172–184.

Muñoz Sierra, Julian D., Oosterkamp, M. J., Wang, W., Spanjers, H., & van Lier, J. B. (2019). Comparative performance of upflow anaerobic sludge blanket reactor and anaerobic membrane bioreactor treating phenolic wastewater: Overcoming high salinity. *Chemical Engineering Journal*, *366*, 480–490.

Muñoz Sierra, Julian David, Lafita, C., Gabaldón, C., Spanjers, H., & van Lier, J. B. (2017). Trace metals supplementation in anaerobic membrane bioreactors treating highly saline phenolic wastewater. *Bioresource Technology*, *234*, 106–114.

Noonari, A. A., Mahar, R. B., Sahito, A. R., & Brohi, K. M. (2019). Anaerobic co-digestion of canola straw and banana plant wastes with buffalo dung: Effect of Fe3O4 nanoparticles on methane yield. *Renewable Energy*, *133*, 1046–1054.

Ozgun, H., Dereli, R. K., Ersahin, M. E., Kinaci, C., Spanjers, H., & Van Lier, J. B. (2013). A review of anaerobic membrane bioreactors for municipal wastewater treatment: Integration options, limitations and expectations. *Separation and Purification Technology*, *118*, 89–104.

Ozyonar, F., & Karagozoglu, B. (2015). Treatment of pretreated coke wastewater by electrocoagulation and electrochemical peroxidation processes. *Separation and Purification Technology*, *150*, 268–277.

Pradeep, N. V., Anupama, S., Navya, K., Shalini, H. N., Idris, M., & Hampannavar, U. S. (2015). Biological removal of phenol from wastewaters: a mini review. *Applied Water Science*, *5*(2), 105–112.

Rafiei, B., Naeimpoor, F., & Mohammadi, T. (2014). Bio-film and bio-entrapped hybrid membrane bioreactors in wastewater treatment: Comparison of membrane fouling and removal efficiency. *Desalination*, *337*(1), 16–22.

Rotaru, A. E., Shrestha, P. M., Liu, F., Markovaite, B., Chen, S., Nevin, K. P., & Lovley, D. R. (2014). Direct interspecies electron transfer between *Geobacter metallireducens* and *Methanosarcina barkeri*. *Applied and Environmental Microbiology*, *80*(15), 4599–4605.

Ryue, J., Lin, L., Liu, Y., Lu, W., McCartney, D., & Dhar, B. R. (2019). Comparative effects of GAC addition on methane productivity and microbial community in mesophilic and thermophilic anaerobic digestion of food waste. *Biochemical Engineering Journal*, *146*, 79–87.

Shin, C., & Bae, J. (2018). Current status of the pilot-scale anaerobic membrane bioreactor treatments of domestic wastewaters: A critical review. *Bioresource Technology*, *247*, 1038–1046. h

Singh, R. K., Kumar, S., Kumar, S., & Kumar, A. (2008). Biodegradation kinetic studies for the removal of p-cresol from wastewater using *Gliomastix indicus* MTCC 3869. *Biochemical Engineering Journal*, *40*(2), 293–303.

Tian, T., Qiao, S., Li, X., Zhang, M., & Zhou, J. (2017). Nano-graphene induced positive effects on methanogenesis in anaerobic digestion. *Bioresource Technology*, *224*, 41–47.

van Lier, J. B., van der Zee, F. P., Frijters, C. T. M. J., & Ersahin, M. E. (2015). Celebrating 40 years anaerobic sludge bed reactors for industrial wastewater treatment. *Reviews in Environmental Science and Biotechnology*, *14*(4), 681–702.

Van Lier, Jules B. (2008). High-rate anaerobic wastewater treatment: Diversifying from end-of-the-pipe treatment to resource-oriented conversion techniques. *Water Science and Technology*, *57*(8), 1137–1148.

Van Lier, Jules B, Mahmoud, N., & Zeeman, G. (2020). *Anaerobic wastewater treatment*.

Veeresh, G. S., Kumar, P., & Mehrotra, I. (2005). Treatment of phenol and cresols in upflow anaerobic sludge blanket (UASB) process: A review. *Water Research*, *39*(1), 154–170.

Villegas, L. G. C., Mashhadi, N., Chen, M., Mukherjee, D., Taylor, K. E., & Biswas, N. (2016). A Short Review of Techniques for Phenol Removal from Wastewater. In *Current Pollution Reports 2*(3), 157–167.

Wang, C., Wang, C., Jin, L., Lu, D., Chen, H., Zhu, W., Xu, X., & Zhu, L. (2019). Response of syntrophic aggregates to the magnetite loss in continuous anaerobic bioreactor. *Water Research*, *164*, 114925.

Wang, W., Han, H., Yuan, M., Li, H., Fang, F., & Wang, K. (2011). Treatment of coal gasification wastewater by a two-continuous UASB system with step-feed for COD and phenols removal. *Bioresource Technology*, *102*(9), 5454–5460.

Wu, B., & Kim, J. (2020). Anaerobic Membrane Bioreactors for Nonpotable Water Reuse and Energy Recovery. *Journal of Environmental Engineering (United States)*, *146*(2), 1–9.

Xie, E., Ding, A., Dou, J., Zheng, L., & Yang, J. (2014). Study on decaying characteristics of activated sludge from a circular plug-flow reactor using response surface methodology. *Bioresource Technology*, *170*, 428–435.

Xu, S., Zhang, W., Zuo, L., Qiao, Z., & He, P. (2020). Comparative facilitation of activated carbon and goethite on methanogenesis from volatile fatty acids. *Bioresource Technology*, *302*, 122801.

Yan, W., Sun, F., Liu, J., & Zhou, Y. (2018). Enhanced anaerobic phenol degradation by conductive materials via EPS and microbial community alteration. *Chemical Engineering Journal*, *352*, 1–9.

Yang, C., Qian, Y., Zhang, L., & Feng, J. (2006). Solvent extraction process development and on-site trial-plant for phenol removal from industrial coal-gasification wastewater. *Chemical Engineering Journal*, *117*(2), 179–185.

Yin, Q., & Wu, G. (2019). Advances in direct interspecies electron transfer and conductive materials: Electron flux, organic degradation and microbial interaction. *Biotechnology Advances*, *37*(8), 107443.

Yin, Q., Yang, S., Wang, Z., Xing, L., & Wu, G. (2018a). Clarifying electron transfer and metagenomic analysis of microbial community in the methane production process with the addition of ferroferric oxide. *Chemical Engineering Journal*, *333*, 216–225.

Yin, Q., Yang, S., Wang, Z., Xing, L., & Wu, G. (2018b). Clarifying electron transfer and metagenomic analysis of microbial community in the methane production process with the addition of ferroferric oxide. *Chemical Engineering Journal*, *333*, 216–225.

Young, L. Y., & Rivera, M. D. (1985). Methanogenic degradation of four phenolic compounds. *Water Research*, *19*(10), 1325–1332.

Zhang, J., Lu, T., Wang, Z., Wang, Y., Zhong, H., Shen, P., & Wei, Y. (2019). Effects of magnetite on anaerobic digestion of swine manure: Attention to methane production and fate of antibiotic resistance genes. *Bioresource Technology*, *291*, 121847.

Zhang, M., Ma, Y., Ji, D., Li, X., Zhang, J., & Zang, L. (2019). Synergetic promotion of direct interspecies electron transfer for syntrophic metabolism of propionate and butyrate with graphite felt in anaerobic digestion. *Bioresource Technology*, *287*, 121373.

Zhao, Q., & Liu, Y. (2016). State of the art of biological processes for coal gasification wastewater treatment. *Biotechnology Advances*, *34*(5), 1064–1072.

Zhao, Z., Li, Y., He, J., & Zhang, Y. (2018). Establishing Direct Interspecies Electron Transfer during Laboratory-Scale Anaerobic Digestion of Waste Activated Sludge via Biological Ethanol-Type Fermentation Pretreatment. *Sustainable Chemistry Engineering*, *6*(10), 13066-13077.

Zhao, Z., Zhang, Y., Holmes, D. E., Dang, Y., Woodard, T. L., Nevin, K. P., & Lovley, D. R. (2016). Potential enhancement of direct interspecies electron transfer for syntrophic metabolism of propionate and butyrate with biochar in up-flow anaerobic sludge blanket reactors. *Bioresource Technology*, *209*, 148–156.

Zhong, D., Li, J., Ma, W., & Xin, H. (2020). Magnetite nanoparticles enhanced glucose anaerobic fermentation for bio-hydrogen production using an expanded granular sludge bed (EGSB) reactor. *International Journal of Hydrogen Energy*, *45*(18), 10664–10672.

Zhou, J., Jiang, S., Yu, H., Wu, C., Zeng, T., Zhou, Y., Hong, Q., & Wang, H. (2020). A comparative study on membrane fouling alleviation mechanisms by using nanoscale Fe_3O_4 and poly dimethyldiallylammonium chloride. *Environmental Technology*, *41*(12), 1477–1485.

Zwietering, M. H., Jongenburger, I., Rombouts, F. M., Van ' K., & Riet, T. (1990). Modeling of the Bacterial Growth Curve Downloaded from. *Applied and Environmental Microbiology*, *56*(6), 1875-1881

Abbreviation:

direct interspecies electron transfer (DIET)
chemical oxygen demand (COD)
mixed liquor suspended solids (MLSS)
anaerobic membrane bioreactor (AnMBR)
organic loading rate (OLR)
coal gasification water treatment plant (CGWTP)
hybrid membrane bioreactors (H-MBR)
membrane bioreactors (MBR)
upflow anaerobic sludge blanket (UASB)
volatile fatty acids (VFAs)
long chain fatty acids (LCFAs)
interspecies electron transfer (IET)
c-type cytochromes (OmcS)
extra cellular substances (EPS)
soluble microbial products (SMPs)
4-hydroxybenzoate (4HBA)
benzoate (BA)
2-bromoethanesulfonate (BES)
volatile suspended solids (VSS)
Specific methane production (SMP)
oxidation reduction potential (ORP)

Appendix

1. Composition of the influent of the AnMBR

Table 1.1 Recipe of metal micronutrients

compound	amount	unit
$FeCl_3.4H_2O$	2	g/L
$CoCl_2.6H_2O$	2	g/L
$MnCl_2.4H_2O$	0.5	g/L
$CuCl_2.2H_2O$	30	mg/L
$ZnCl_2$	50	mg/L
HBO_3	50	mg/L
$(NH_4)6Mo_7O_{24}H_2O$	90	mg/L
$Na_2SeO_3.5H_2O$	100	mg/L
$NiCl_2.6H_2O$	50	mg/L

Table 1.2 Recipe of metal macronutrients

compound	amount	unit
NH_4Cl	170	g/L
$CaCl_2.2H_2O$	8	g/L
$MgSO_4.7H_2O$	9	g/L

Table 1.3 Addition of other compounds

compound	amount	unit
Acetate	g/L	4.26
NaCl	g/L	18.3

2. Addition of chemicals of batch experiments

Table 2.1 Addition of chemicals in batch experiments

	BES (mmol/L)	Magnetite (mmol/L)	Na BES (g/L)	NaCl (g/L)	Na BES (g/80mL)	NaCl (g/80mL)	magnetite (g/80mL)
control	0	0	0.000	2.923	0.000	0.234	0
bes	50	0	10.551	0.000	0.844	0.000	0
mag	0	20	0.000	2.923	0.000	0.234	0.370
BesMag	50	20	10.551	0.000	0.844	0.000	0.370

3. Python code of curve fit (model of *p*-cresol control group using both Gompertz and Logistic as an example)

```
%matplotlib inline
import numpy as np
import matplotlib.pyplot as plt
import pandas as pd
from scipy.optimize import curve_fit
from scipy.stats import pearsonr

pcresol = pd.read_excel('p-cresol+benzoate.xlsx', sheet_name = 'pcresol', header =
[0,1])

#Gompertz model
def func(t, S0, Rm, Lambda): #Rm is the maximum substrate transformation rate, in
mg*L-1 d-1, Lambda is the lag phase, in d
    y = S0 * (1 - np.exp(-np.exp((Rm * np.exp(1))*(Lambda - t)/S0 + 1)))
    return y

#Logistic model
def Logistic(t, S0, Rm, Lambda): #Rm is the maximum substrate transformation rate,
in mg*L-1 d-1, Lambda is the lag phase, in d
    y = S0 * (1 - 1 / (1 + np.exp(4 * Rm * (Lambda - t) / S0 + 2)))
    return y
```

```
plt.figure(figsize=(20,15))
plt.subplot(321)
xdata = pcresol.index
ydata = pcresol.pcresol.control
popt, pcov = curve_fit(func, xdata, ydata, p0 = [250, 80, 10])
print(popt)

ax1 = plt.subplot(3,2,1)
plt.plot(xdata, func(xdata, *popt), 'g--', label = 'modelled data')      #modelled data
plt.plot(xdata,ydata, marker = 'o')                                       #observed data
plt.title('pcresol-Gompertz-control')
plt.legend(loc='best')
plt.xlabel('day')
plt.ylabel('concentration(mg/L)')
corr_pcresol = pearsonr(ydata, func(xdata, *popt))
print('corr_pcresol is', corr_pcresol)

plt.figure(figsize=(20,15))
plt.subplot(321)

xdata = pcresol.index
ydata = pcresol.pcresol.control
popt, pcov = curve_fit(Logistic, xdata, ydata, p0 = [250, 80, 10])
print(popt)
ax6 = plt.subplot(3,2,1)
plt.plot(xdata, Logistic(xdata, *popt), 'g--', label = 'modelled data') #modelled data
plt.plot(xdata,ydata, marker = 'o')                                       #observed data
plt.title('pcresol-Log-control')
plt.legend(loc='best')
plt.xlabel('day')
plt.ylabel('concentration(mg/L)')
log_pcresol = pearsonr(ydata, Logistic(xdata, *popt))
print('log_pcresol is', log_pcresol)
```

4. batch experiment 1 and 2 substrate degradation

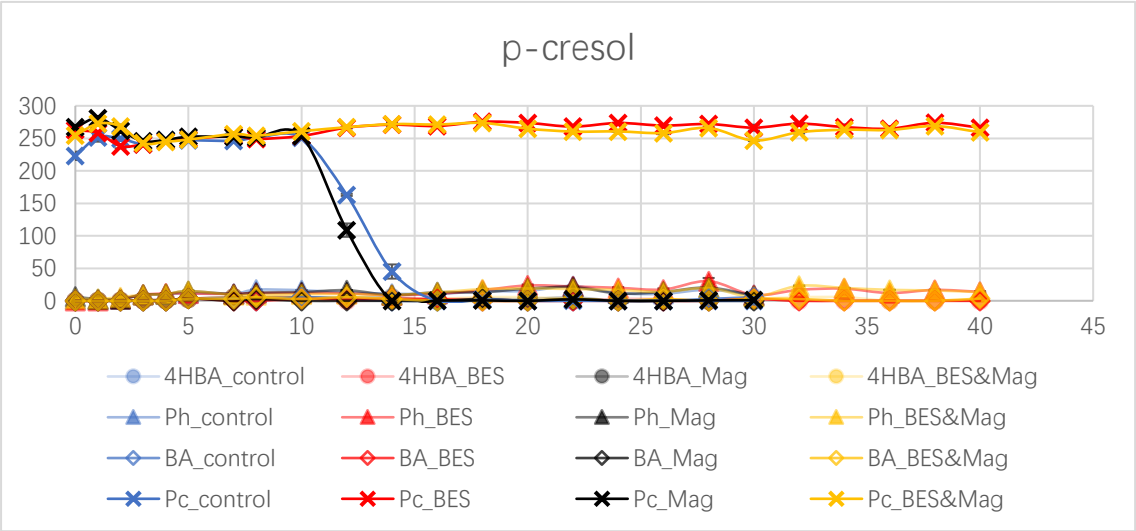

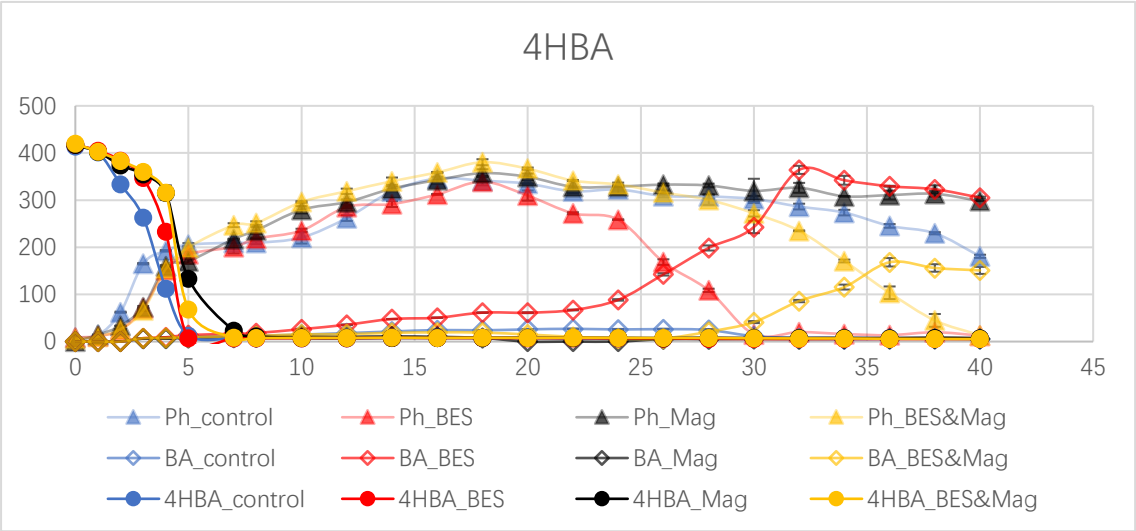

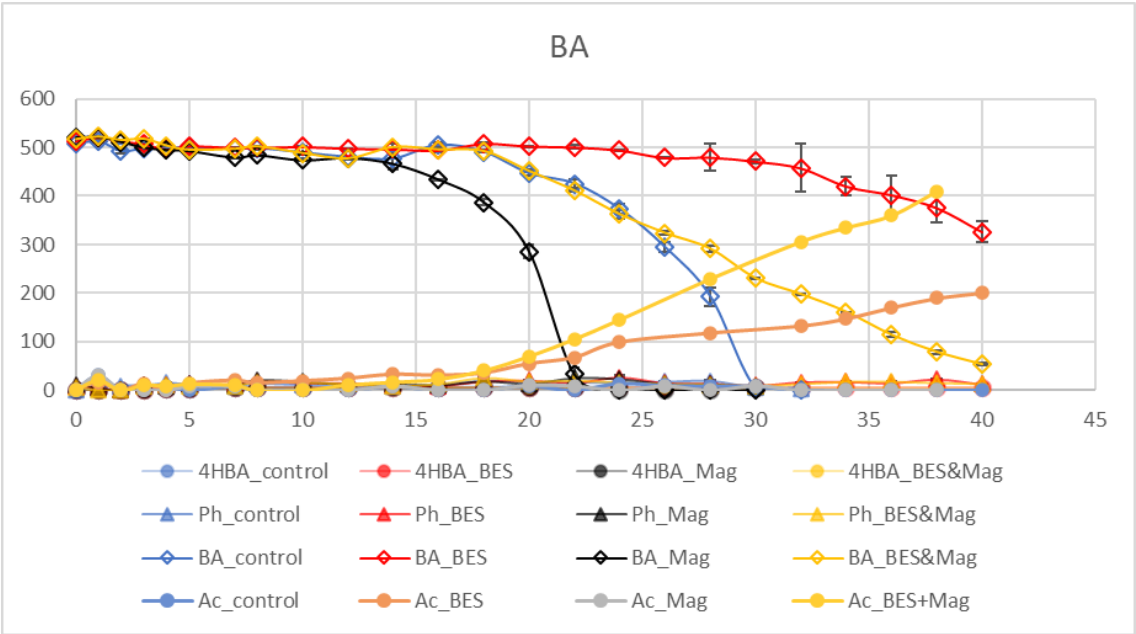

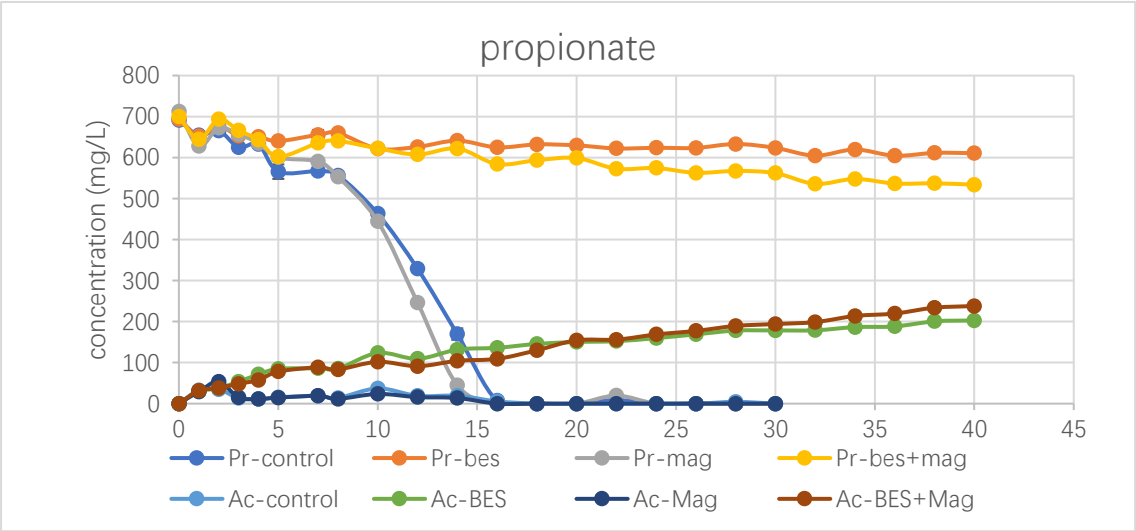

Figure 4.1. Batch experiment 1 substrate degradation with intermediates in the same graph
4HBA: 4-hydroxybenzoate,
BA: benzoate,
Ph: phenol,
Pr: propionate,
Ac: acetate

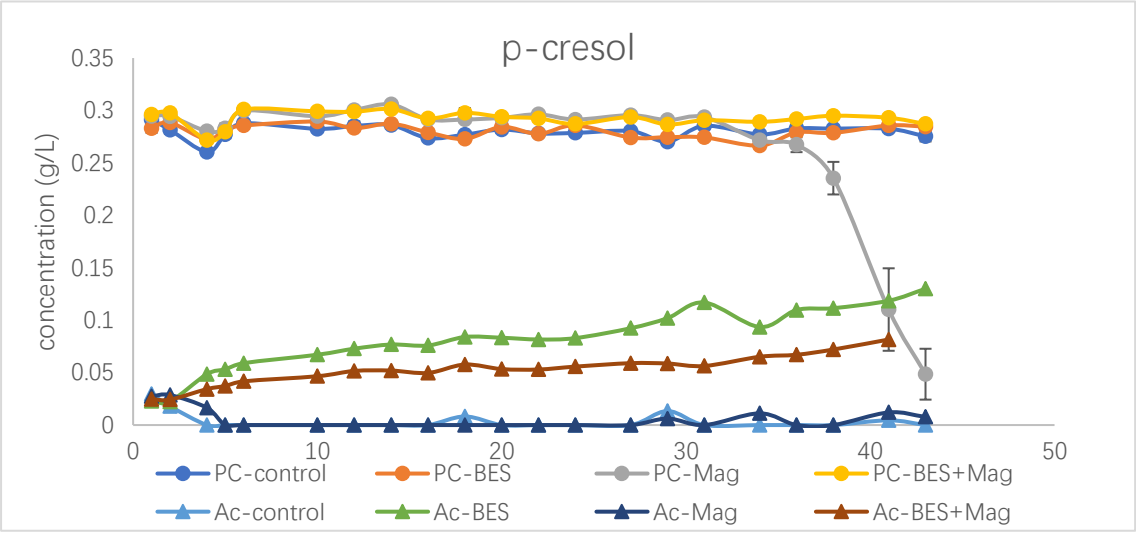
p-cresol
concentration (g/L)
0.35
0.3
0.25
0.2
0.15
0.1
0.05
0
0
10
20
30
40
50
PC-control
PC-BES
PC-Mag
PC-BES+Mag
Ac-control
Ac-BES
Ac-Mag
Ac-BES+Mag

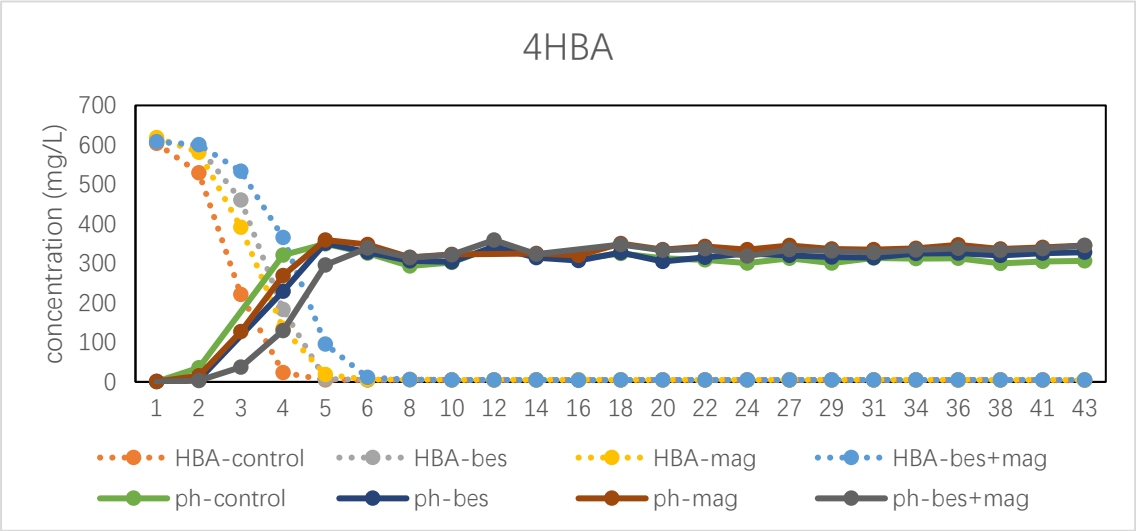
4HBA
concentration (mg/L)
700
600
500
400
300
200
100
0
1 2 3 4 5 6 8 10 12 14 16 18 20 22 24 27 29 31 34 36 38 41 43
HBA-control
HBA-bes
HBA-mag
HBA-bes+mag
ph-control
ph-bes
ph-mag
ph-bes+mag

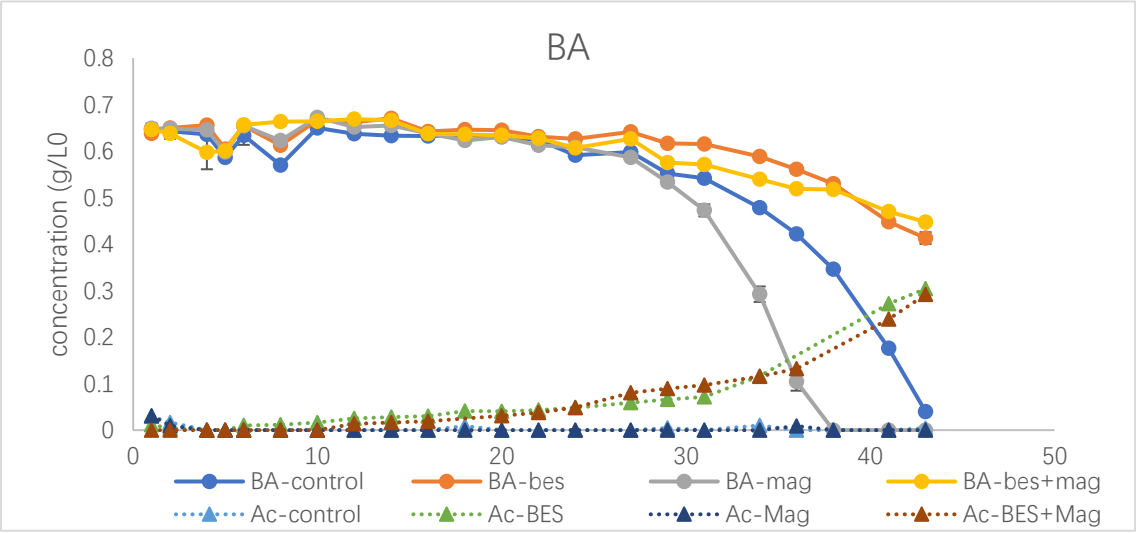
BA
concentration (g/L0
0.8
0.7
0.6
0.5
0.4
0.3
0.2
0.1
0
0
10
20
30
40
50
BA-control
BA-bes
BA-mag
BA-bes+mag
Ac-control
Ac-BES
Ac-Mag
Ac-BES+Mag

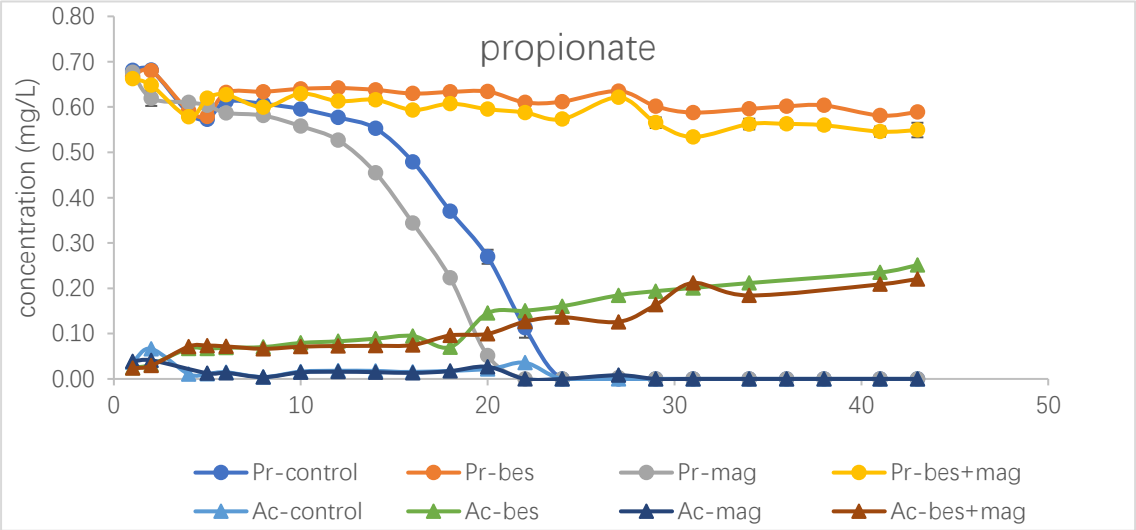

Figure 4.2 Batch experiment 2 substrate degradation with intermediates in the same graph

4HBA: 4-hydroxybenzoate,

BA: benzoate,

Ph: phenol,

Pr: propionate,

Ac: acetate

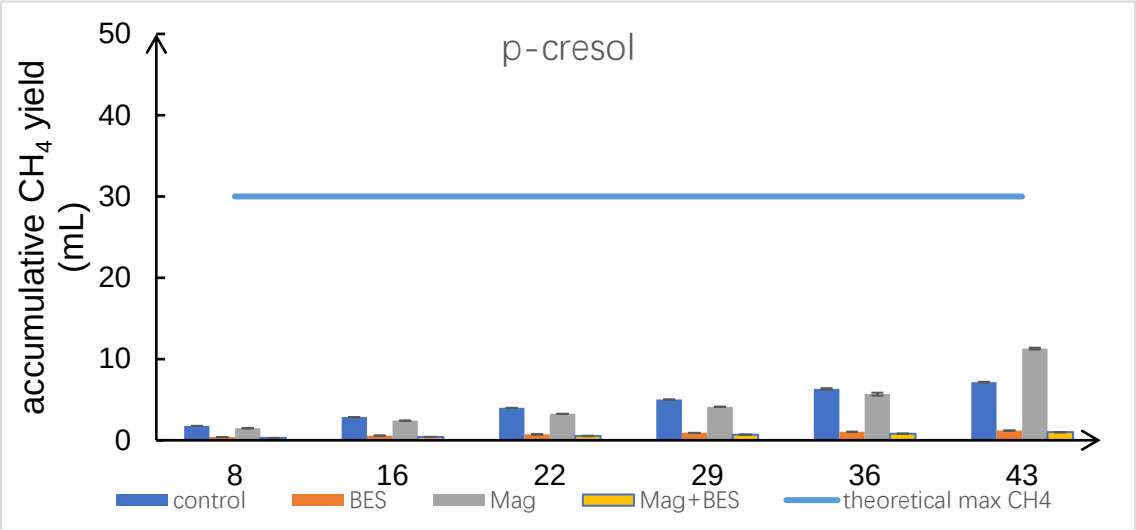
p-cresol
accumulative CH4 yield (mL)
50
40
30
20
10
0
8
16
22
29
36
43
control
BES
Mag
Mag+BES
theoretical max CH4

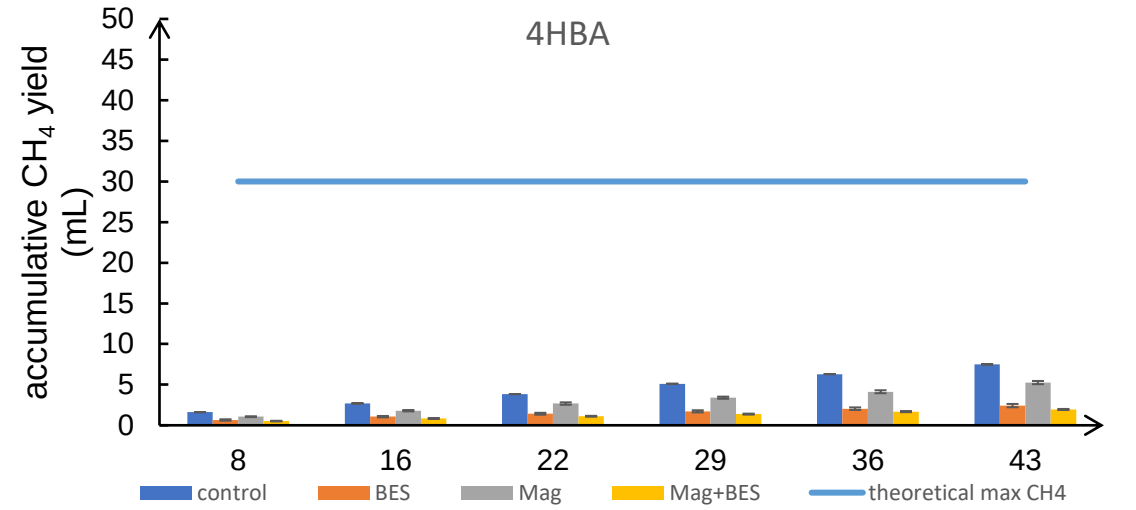
4HBA
accumulative CH4 yield (mL)
50
45
40
35
30
25
20
15
10
5
0
8
16
22
29
36
43
control
BES
Mag
Mag+BES
theoretical max CH4

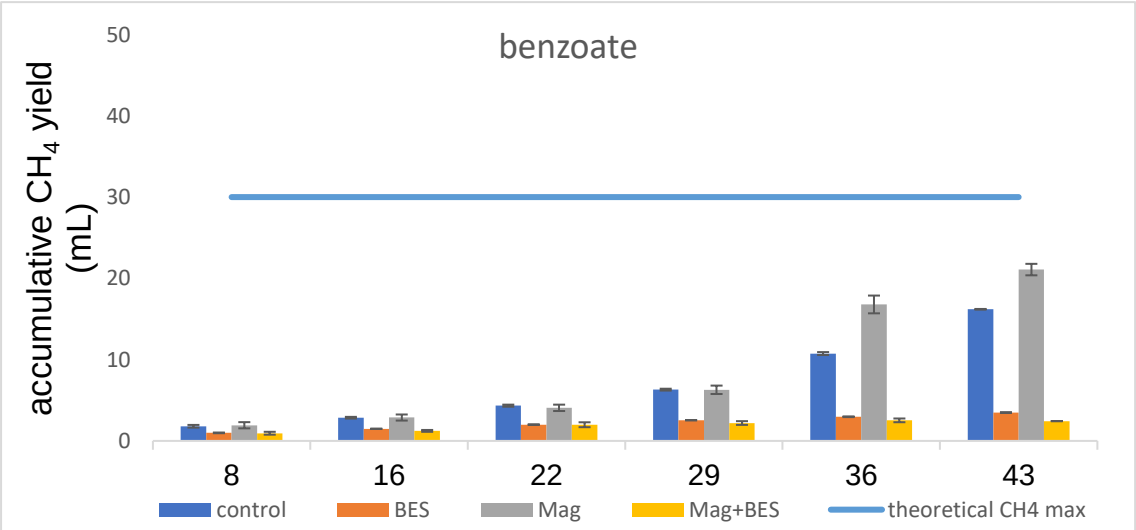
benzoate
accumulative CH4 yield (mL)
50
40
30
20
10
0
8
16
22
29
36
43
control
BES
Mag
Mag+BES
theoretical CH4 max

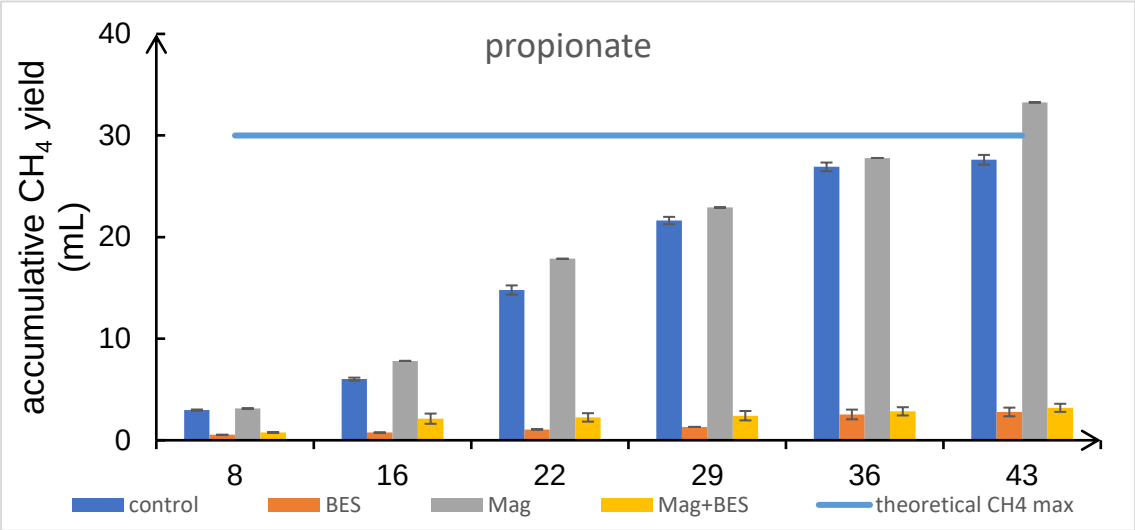

Figure 4.3 Methane production in batch experiment 2

5. COD balance of batch experiment 1 and 2

Table 5.1. COD balance of batch experiment 1

No.	trial condition	COD balance
1	pcresol-control	0.966171
3	pcresol-BES	0.905135
5	pcresol-Mag	0.987504
7	pcresol-BES&Mag	0.885895
9	4HBA-control	0.740891
11	4HBA-BES	0.847241
13	4HBA-Mag	0.866352
15	4HBA-BES&Mag	0.8653
17	benzoate-control	0.862222
19	benzoate-BES	0.876202
21	benzoate-Mag	0.906128
23	benzoate-BES&Mag	0.842988
25	phenol-control	0.847776
27	phenol-BES	0.886189
29	phenol-Mag	0.815406
31	phenol-BES&Mag	0.896424
33	propionate-control	0.843714
35	propionate-BES	0.834834
37	propionate-Mag	0.998501
39	propionate-BES&Mag	0.855421

Table 5.2. COD balance of batch experiment 2

No.	trial condition	COD balance
1	pcresol-control	1.20356
3	pcresol-BES	0.977794
5	pcresol-Mag	0.521988
7	pcresol-BES&Mag	0.950843
9	4H-control	1.14149
11	4H-BES	0.963147
13	4H-Mag	1.165161
15	4H-BES&Mag	0.958709
17	benzoate-control	0.620146
19	benzoate-BES	0.957417
21	benzoate-Mag	0.620214
23	benzoate-BES&Mag	0.945496
25	phenol-control	0.999655
27	phenol-BES	0.953101
29	phenol-Mag	0.98661
31	phenol-BES&Mag	0.93438
33	propionate-control	0.715676
35	propionate-BES	0.876518
37	propionate-Mag	0.786674
39	propionate-BES&Mag	0.883723

6. ORP of the reactor

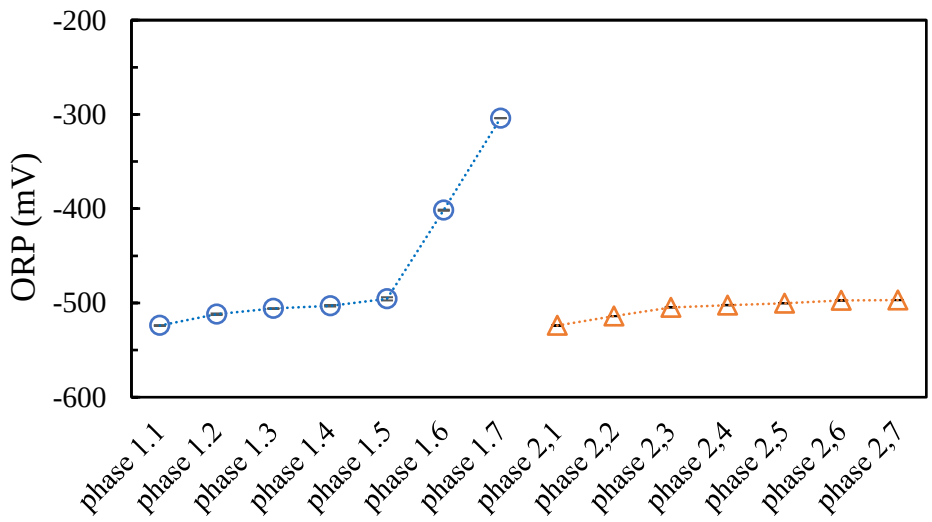

Figure 6.1 Change of ORP in the AnMBR